nature microbiology

Article

https://doi.org/10.1038/s41564-026-02310-w

Community context reshapes microbial proteomes and reduces functional overlap

Received: 11 September 2025

Accepted: 27 February 2026

Published online: 24 April 2026

Check for updates

Sarah Moraïs[1,2,3], Michael Mazor[1,2,3], Itai Amit[1,2,3], Philip Gerth[4], Anke Trautwein-Schult[4], Sandra Maaß[4], Ido Grinshpan[1,2,3], Yehonatan Shelly[1,2,3], Liron Levin[5], Dörte Becher[4] & Itzhak Mizrahi[1,2,3]

Microbial coexistence in complex communities requires mechanisms that minimize competition and optimize resource use. However, the mechanisms by which these ecological strategies are executed remain poorly understood. Here we show that bacteria modulate protein abundance in response to specific community members, reducing functional redundancy and promoting metabolic complementarity. Using synthetic gut-derived consortia exposed to distinct carbon sources, we systematically profiled proteomic responses of individual species across isolate, pairwise and 4-member communities. We found that biotic interactions, rather than abiotic conditions, were the dominant drivers of proteomic variation. These interactions led to reproducible, partner-specific expression shifts that significantly reduced functional overlap and were frequently associated with increased community productivity. Together, these findings highlight gene expression as a means by which microbes implement ecological strategies in community contexts. Through this regulatory plasticity, microbes dynamically reshape their realized niche through protein abundance modulation, enabling them to partition metabolic space and stabilize community structure.

Microbial communities are integral components of all ecosystems on Earth, playing crucial roles in nutrient cycling, energy flow and overall ecosystem functionality[1–3]. Similar to most organisms in nature, microbes live in complex multispecies communities and are subject to ecological forces that shape their structure and dynamics. Across ecosystems, organisms that coexist in such communities often partition ecological niches to reduce direct competition, giving rise to trophic interaction networks built on functional complementarity[4,5]. Microbes are no exception, exhibiting clear preferences for specific nutrients, and well-documented specialization for distinct carbon sources often resulting in cross-feeding interactions[6,7]. Indeed, complex interdependencies among microbial species have been widely observed[8,9], enhancing survival under stress, improving resource utilization, and contributing to ecosystem resilience[10–12]. While cooperative behaviours such as metabolic exchange[13] and quorum sensing[14] have been described, the prevailing view is that competition remains a dominant force shaping microbial communities across diverse environments[15]. However, this view is complicated by several inherent features of microbes. One such feature is their remarkable metabolic flexibility, which allows them to exploit alternative resources and occupy dynamic niches, often by utilizing metabolites excreted by other species[16]. This capacity may also provide a resolution to longstanding ecological puzzles such as the paradox of the plankton, by enabling species to coexist despite apparent overlap in resource use[17]. These characteristics

[1]National Institute of Biotechnology in the Negev, Ben-Gurion University of the Negev, Be'er Sheva, Israel. [2]Department of Life Sciences, Ben-Gurion University of the Negev, Be'er Sheva, Israel. [3]The Goldman Sonnenfeldt School of Sustainability and Climate Change, Ben-Gurion University of the Negev, Be'er Sheva, Israel. [4]Institute of Microbiology, Department of Microbial Proteomics, Center for Functional Genomics of Microbes, University of Greifswald, Greifswald, Germany. [5]Bioinformatics Core Facility, Ilse Katz Institute for Nanoscale Science and Technology, Ben-Gurion University of the Negev, Beer-Sheva, Israel. e-mail: imizrahi@bgu.ac.il

challenge overly simplistic models of microbial interaction and underscore the need for a deeper understanding of the ecological principles that govern microbial coexistence. By elucidating the mechanisms that promote stability, structure and coexistence in microbial communities, we can better harness their ecological potential and develop strategies to predict, design and control microbial systems.

Another inherent feature of microbes is their capacity for rapid sensing and adaptation. In natural environments, microbes predominantly exist as single cells and must continually monitor and respond to fluctuations in their surroundings. To this end, they have evolved intricate sensing and regulatory systems that allow them to swiftly alter their behaviour through dynamic changes in gene expression[18]. Modulation of gene expression in response to abiotic factors, such as temperature, pH or nutrient availability, is a well-established microbial strategy for environmental adaptation. A classical example is the lactose operon, in which gene expression is tightly regulated by the presence or absence of specific metabolites, enabling efficient carbon utilization under appropriate conditions[19]. While extensive research has examined how microbes respond to abiotic stimuli, much less is known about how they adjust gene expression in response to their biotic environment, particularly the presence of other microbial species. This is especially relevant in the context of niche theory; in classical ecology, the realized niche represents the actual conditions and resources an organism utilizes in the presence of competitors and environmental constraints, distinguished from the fundamental niche, which encompasses the full range of conditions it could theoretically exploit in the absence of such limitations[20]. In microbial systems, this concept can be mechanistically grounded in protein abundance: the realized niche reflects the subset of an organism's genetic potential that is actively expressed in response to current abiotic and biotic conditions. Thus, protein abundance profiles provide a direct molecular readout of the realized niche, as it is shaped by interactions and environmental inputs. We hypothesized that microbial regulatory plasticity may play a role in mediating ecological interactions, potentially enabling microbes to reduce direct competition, expand into new metabolic niches, or exploit cross-feeding opportunities created by neighbouring species. This led us to ask: do microbes alter protein abundance in response to specific community members? And are these responses species-specific, or do they follow generalizable patterns across taxa and environments? Answering these questions is essential for understanding how gene regulation contributes to microbial coexistence, niche partitioning and the formation of trophic networks in complex ecosystems.

To address these questions, we employed a systematic, bottom-up approach to investigate microbial interaction dynamics in controlled communities exposed to two distinct carbon source environments. We examined a set of bacterial species as single isolates under each abiotic condition and progressively assembled more complex communities, including pairwise combinations and 4-member consortia. This experimental design enabled us to precisely track changes in the proteomic profiles of each species in response to either carbon source identity or the presence of microbial counterparts. Our results reveal a general pattern: in the presence of other microbes, species consistently alter their proteomic profiles in a partner-dependent manner. These expression changes are closely associated with a reduction in functional overlap within the community. Moreover, our data show that biotic interactions are the dominant explanatory variable in protein abundance variance and, in many cases, are also linked to increased productivity. Together, these findings reinforce the view that microbes in nature predominantly exist and operate within complex interactive communities, where regulatory flexibility may help minimize competition. By uncovering reproducible patterns of protein abundance modulation driven by community context, our study reveals fundamental principles that govern microbial coexistence and functional organization in diverse ecosystems.

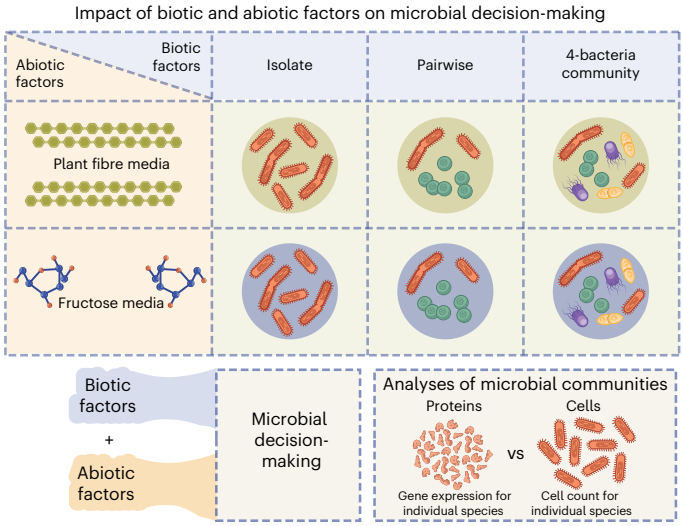

Fig. 1 | Experimental setup for examining the impact of biotic and abiotic factors on microbial gene expression and community productivity. To disentangle the effects of biotic (columns) and abiotic (rows) factors, we analysed protein expression profiles and growth of individual isolates, their pairwise combinations, and two distinct 4-member communities. These were cultivated in two contrasting carbon source environments, plant fibre and fructose media, representing abiotic variation. This design enabled a systematic assessment of how community composition (biotic) and nutrient environment (abiotic) influence microbial proteomes and overall community productivity, as measured by species-specific cell counts and protein expression (bottom).

Results

Comparing the impact of biotic and abiotic factors on protein abundance

In our experimental setup, we aimed to investigate the influence of both abiotic and biotic factors on protein abundance and biomass production across a set of bacterial strains. We selected two distinct carbon sources as abiotic factors: fructose and ground wheat straw (a complex plant fibre). These carbon sources were also selected as they differ in chemical complexity (simple and complex polysaccharides) to create diverse community structures while maintaining the same initial bacterial diversity (Fig. 1). In addition, we examined the effect of biotic factors by culturing each bacterium either as an isolate or within communities of varying richness (1, 2 or 4 species). This approach allowed us to explore how differences in environmental conditions, community composition and richness influence bacterial interactions, protein abundance and biomass production. Given that a substantial portion of cellular energy is allocated to protein production, and that bacteria tightly regulate this process to optimize efficiency[21–23], we used proteomics to profile protein abundance. This approach offers a realistic view of the proteins actually produced and enables quantitative estimates, providing insights that transcriptomic methods alone often fail to capture. To ensure high-resolution proteomic profiling of all consortium members within the detectable limit per sample[24], we assembled synthetic minimal consortia, comprising a limited number of bacterial species (up to 4 per consortium). We selected a diverse array of bacteria with varying phylogenetic backgrounds and functional traits[25], aiming to emulate gut ecosystems (human or rumen) and represent the typical trophic layers found in such environments[26]. The synthetic consortia approach is also advantageous for its capacity to conduct comprehensive investigations into molecular, proteomic and microscopic dimensions, owing to the controlled number of bacteria incorporated. In the first consortium, we assembled all pairwise combinations and the full 4-member community comprising metabolically distinct human gut-associated species. *Eubacterium hallii* is a versatile anaerobe that ferments glucose

https://doi.org/10.1038/s41564-026-02310-w

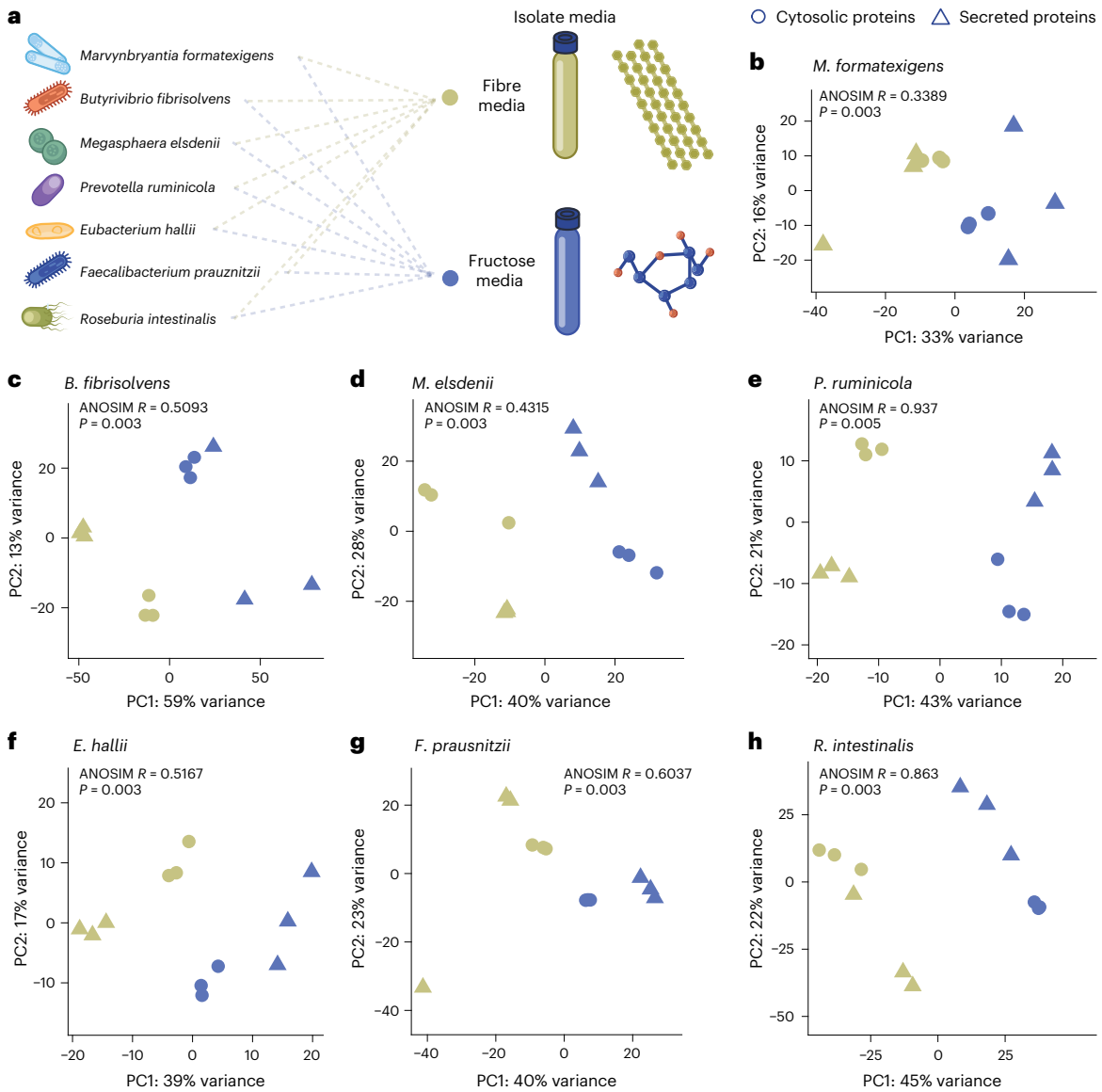

Fig. 2 | Proteome expression is modulated by the environment. a, Seven bacteria were cultivated as isolates on both fructose or fibre as carbon source (3 biological replicates). **b**–**h**, PCA of the overall proteomes for each of the indicated bacteria (LFQ values), colour coded by the carbon source (blue for fructose and green for fibre); shapes indicate cytosolic or secreted proteins (pellets or supernatant fractions). Clustering analysis of expressed proteins according to the carbon source was performed using ANOSIM (two-sided) with 10,000 randomizations of the data, and the resulting *R* and *P* value corrected using the FDR Benjamini–Hochberg method are indicated.

and lactate into butyrate and hydrogen, and can utilize glycerol to produce 1,3-propanediol[27]. *Roseburia intestinalis* degrades hemicellulose and starch, producing butyrate as a terminal metabolite, and is frequently associated with dietary fibre metabolism[28]. *Marvinbryantia formatexigens* specializes in degrading amorphous cellulose and produces formate and acetate as fermentation end products[29]. *Faecalibacterium prausnitzii* is a prominent butyrate producer with proposed anti-inflammatory effects[30]. In the second consortium, we constructed all pairwise and full combinations of 4 representative bovine rumen species. *Prevotella ruminicola* is a dominant hemicellulolytic and peptide-utilizing fermenter that breaks down xylans and starches, generating succinate and propionate[31]. *Butyrivibrio fibrisolvens* hydrolyses hemicellulose and pectin, producing butyrate and lactate[32]. *Megasphaera elsdenii* is a lactate- and sugar-utilizing bacterium that plays a key role in stabilizing ruminal fermentation by converting lactate to propionate and butyrate[33]. *E. hallii* was also included in this consortium due to its cross-system metabolic relevance and ability to integrate fermentation intermediates into butyrate synthesis.

The assembled communities were analysed across both abiotic and biotic dimensions. Carbon source conditions were used to assess abiotic effects, while comparisons to single-species isolates allowed us to evaluate biotic influences on protein expression and cell abundance (Fig. 1).

Proteome profile is modulated by both environment and microbial composition

Initially, we examined both the growth and proteome expression of individual bacteria when cultured on the two different carbon sources (abiotic change). While growth was largely unaffected by the change in carbon source in most cases (Extended Data Fig. 1), proteome expression showed a strong response to this change (Fig. 2). Principal-component analyses (PCA) of protein abundance of each bacterial species exhibited discrete and individual response to carbon

https://doi.org/10.1038/s41564-026-02310-w

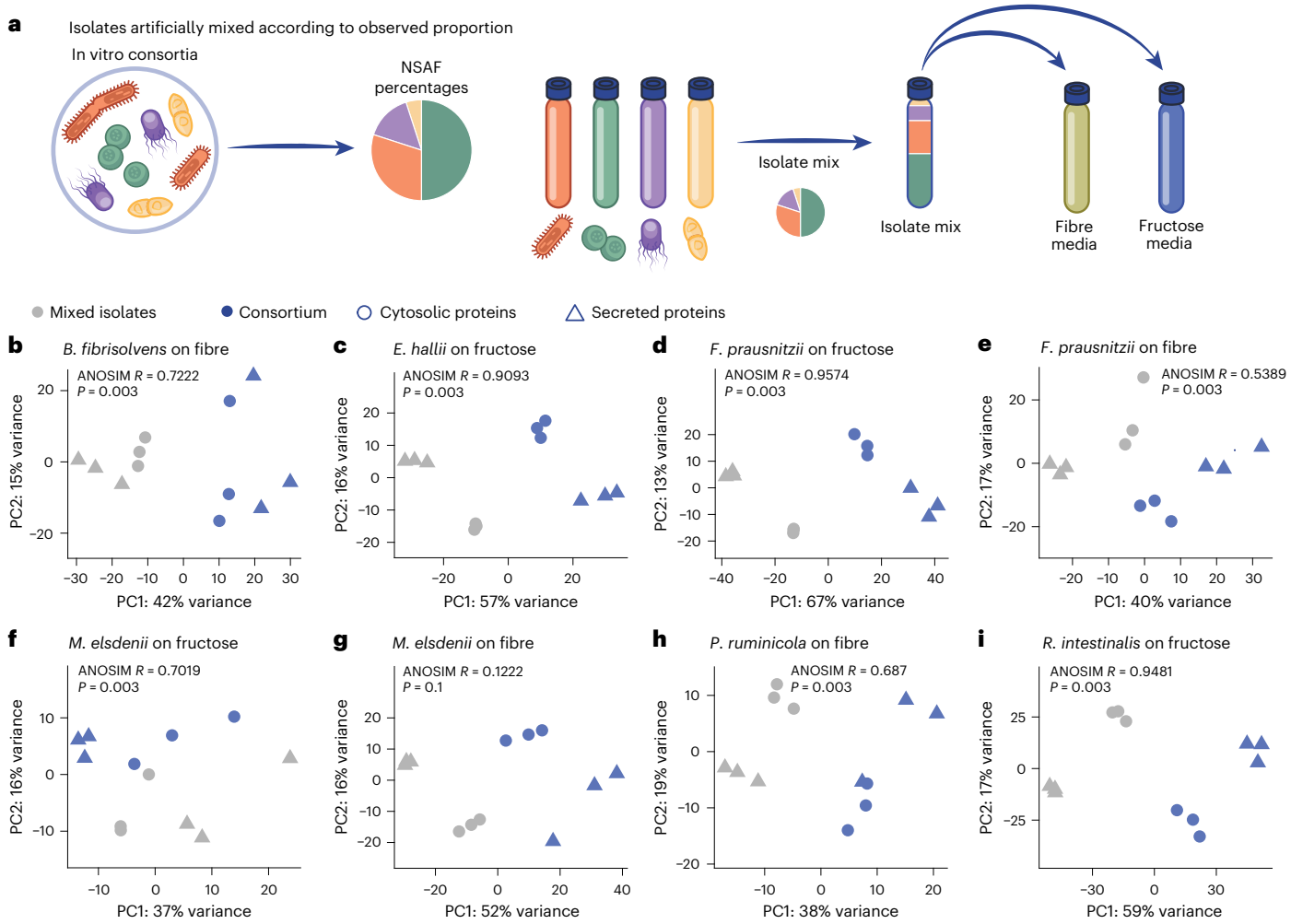

Fig. 3 | Microbial proteomes are actively reshaped in response to community context. a, Schematic representation of the experimental design. Four-species consortia were assembled by mixing equal ratios (1:1) of each species and grown for 24 h on either plant fibre or fructose media (3 biological replicates). For each species, proteome and community composition were determined. Relative species-specific proteome abundances (NSAF values) were then used to generate mixed-isolate controls by proportionally combining the proteomes of the same strains grown individually. These mixed-isolate controls were analysed in the same way as the self-assembled communities, allowing direct comparison of species-specific expression profiles while avoiding the depth and coverage limitations typically associated with complex community proteomics. **b**–**i**, PCA of total proteomes for each indicated species (LFQ values) under the two carbon source conditions, comparing self-assembled consortia (blue) with mixed-isolate controls (grey); shapes indicate cytosolic or secreted proteins (pellet or supernatant fractions). Clustering by culture type was assessed using ANOSIM (two-sided) with 10,000 permutations; *R* and *P* values corrected using the FDR Benjamini–Hochberg method are shown. These analyses reveal that proteomes are modulated by community context, with species-specific expression patterns emerging only in live, self-assembled consortia.

changes (analysis of similarities (ANOSIM) $0.3389 < R < 1, P = 0.1$). Clustering was primarily driven by the first principal component (PC1), which accounted for 33–59% of the variance in protein abundance across individual microbes. Such changes in protein expression upon varying media composition are consistent with previous reports in individual cultures[34–37].

To investigate whether (1) microbes alter their proteomes in response to other community members, (2) such responses are specific to particular counterparts, and (3) generalizable patterns underlie these changes, we analysed all assembled 2-species and 4-species consortia, examining proteome expression across both biotic and abiotic dimensions. Specifically, each consortium was grown under two distinct carbon sources, fructose and fibre, to assess abiotic effects, and compared to corresponding single-species cultures to evaluate biotic influences (Fig. 1). To address limitations in proteomic depth and coverage inherent to complex communities, we generated mixed isolate controls for the 4-species consortia. These mixes reflected the observed community structure (Extended Data Fig. 2) and were analysed alongside the grown consortia to enable direct comparison of proteomic profiles (Fig. 3a, Extended Data Fig. 3, Supplementary Table 1 and Methods). To ensure robust and comparable measurements, we included only those microbes with higher than 5% of the relative abundance and with at least 400 proteins detected per genome across all tested conditions. Six of the seven tested species met these criteria and were retained for further analysis. These species yielded sufficiently rich proteomic data to assess their responses to community environments compared to growth in isolation. This setup allowed us to compare the proteome of each species in isolation versus within a consortium and in the cases of *M. elsdenii* and *F. prausnitzii*, on both carbon source conditions (Fig. 3). Across all comparisons, we observed significant changes in protein expression for each species when grown in isolation compared to when grown in consortia (Fig. 3b), whereas growth differences alone were not necessarily statistically significant (Extended Data Fig. 4). Moreover, here the majority of the variance in response to biotic conditions was reflected on PC1 axes with 37–67% of the variance per microbe. The clear clustering of all

https://doi.org/10.1038/s41564-026-02310-w

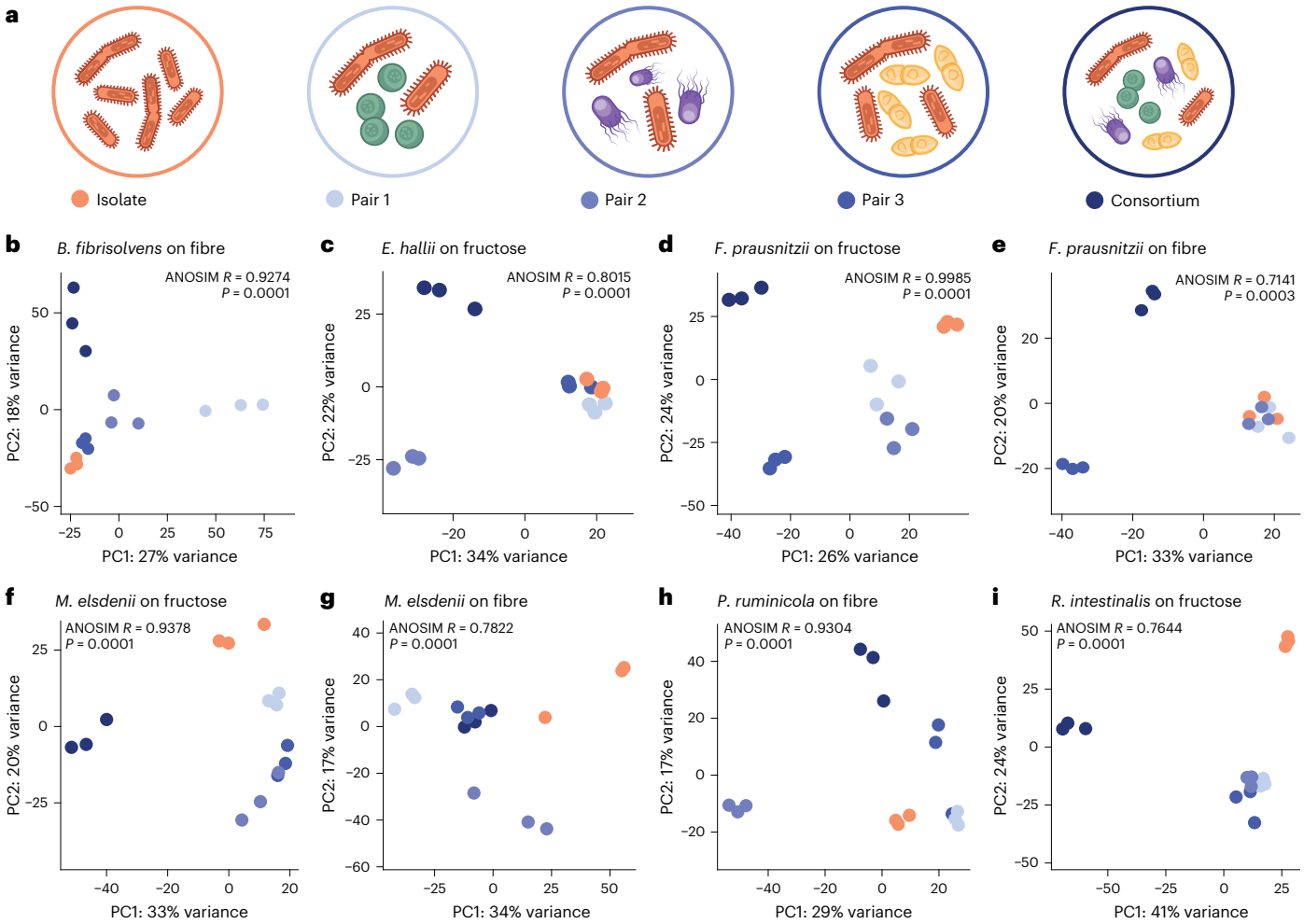

Fig. 4 | Species-level proteomic responses are shaped by community context. **a**, Species-level proteomics were analysed for individual species, 3 different pairs and the consortia of 4 bacterial species. **b**–**i**, PCA of the overall cytosolic proteins (secreted proteins PCA are available in Supplementary Fig. 5) for each of the indicated bacteria (LFQ values) and carbon source in the communities described in **a** (3 biological replicates) (with corresponding colour coding). Clustering analysis of expressed proteins according to the type of culture was performed using ANOSIM with 10,000 randomizations of the data, and the resulting *R* and *P* value corrected using the FDR Benjamini–Hochberg method are indicated. The total biomass produced in these contexts by each bacterium is available in Supplementary Fig. 4.

biological replicates for each biotic condition further emphasizes that the proteomic response is highly constrained and reproducible (most $P < 0.01$; Fig. 3b). Taken together, these findings indicate that microbes respond in a consistent and reproducible manner to the same community composition.

Bacteria respond in a specific manner to specific counterparts

Following the consistent protein expression patterns observed in individual populations in response to the same community composition, we further examined how specific and distinguishable these responses are to different microbial counterparts. We found that for each bacterium, distinct and reproducible patterns of proteomic shifts emerged across replicates when paired with different partners in co-cultures (Fig. 4 and Extended Data Fig. 5), suggesting that bacteria respond in a specific manner to specific counterparts. In most cases, these pairwise interaction patterns were distinct from those observed when the same microbes were grown either in larger consortia or in isolation (Fig. 4 and Extended Data Fig. 5). Intriguingly, while some bacteria, such as *F. prausnitzii* grown on fructose (Fig. 4d), exhibited clear and distinct proteomic profiles depending on the partner or community context, others showed more generalized responses. For instance, *F. prausnitzii* grown on fibre displayed similar expression patterns across different pairwise combinations, which clustered more closely together compared with those observed in the 4-member consortia (Fig. 4e).

Furthermore, in the case of *E. hallii* grown on fibre, we could compare its proteomics changes across 6 different pairwise consortia, and all exhibited significantly distinct patterns, further emphasizing the profound responses of the proteomes to microbial community changes (Extended Data Fig. 6). To investigate these proteomic changes at the Kyoto Encyclopedia of Genes and Genomes (KEGG) Orthology (KO) level, we categorized each KO within a consortium as either unchanged or modulated, and examined their distribution across the global metabolic map (KEGG map1100). We found that both unchanged and modulated KOs were broadly distributed across the metabolic landscape, with no single pathway consistently enriched in either category (Extended Data Fig. 7). This widespread distribution highlights that proteomic shifts are not restricted to specific functions, but rather reflect a broad, dynamic adjustment of the bacterial proteome in response to changes in environmental conditions or community composition. The fact that we did not identify any consistent or recurring patterns of pathway modulation across the various communities we analysed suggests that each microbial species adopts a distinct strategy for proteome modulation in response to different community contexts.

https://doi.org/10.1038/s41564-026-02310-w

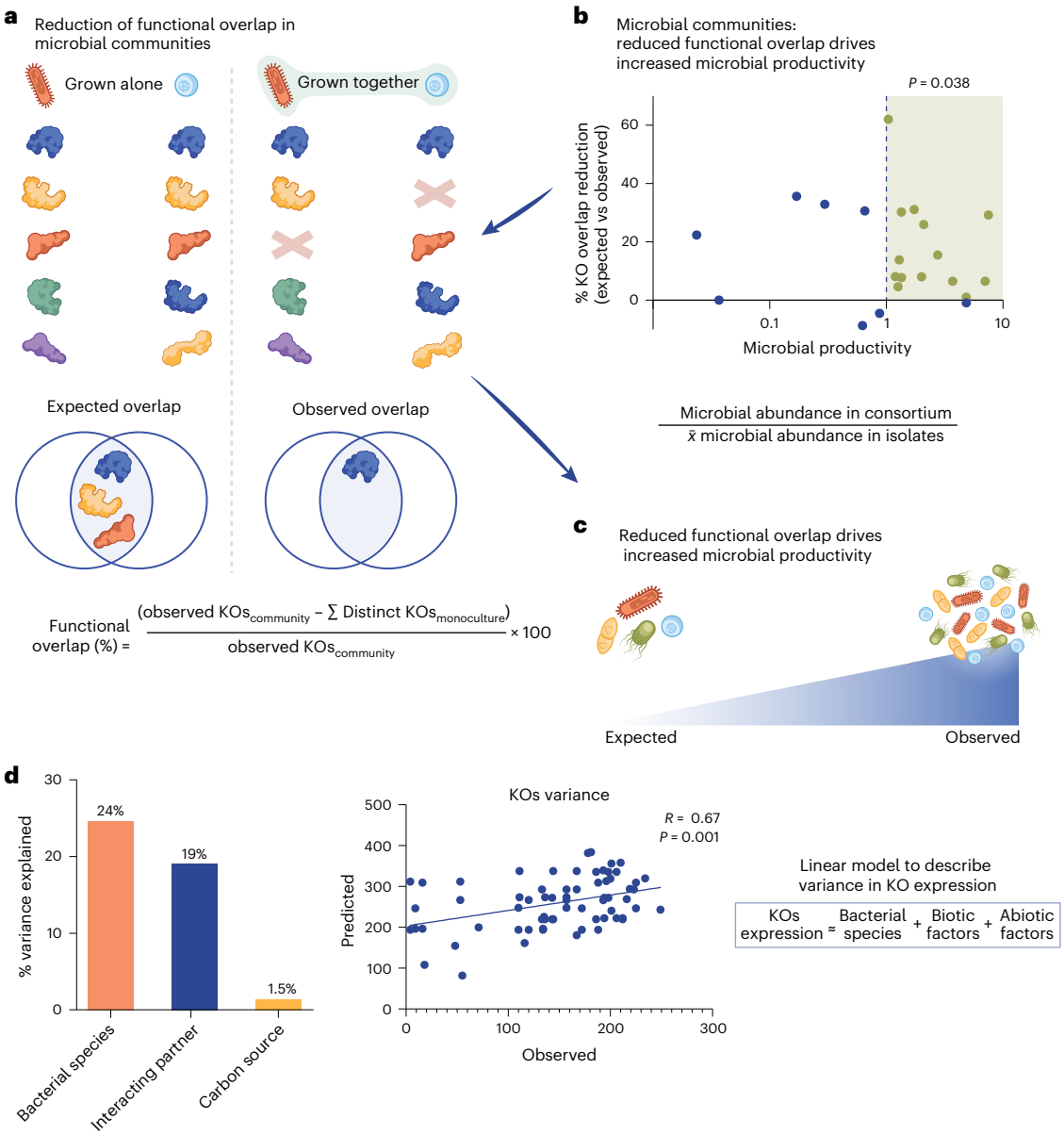

Fig. 5 | Functional overlap reduction in microbial communities is coupled with enhanced productivity. a, Schematic illustration of functional redundancy and the calculation method used for percent KO overlap reduction (genomic potential not considered). **b**, Scatterplot showing the relationship between percent KO overlap reduction (*y* axis, NSAF presence/absence) and community productivity (*x* axis). Communities exhibiting reduced functional redundancy alongside increased productivity are highlighted in green; odds ratio (OR) = 9.75; Wald test one-sided $P = 0.038$. Each dot represents the mean of 3 biological replicates. **c**, Conceptual schematic illustrating that reduced functional overlap in microbial communities is associated with enhanced productivity. **d**, Left: bar plot displaying the proportion of variance in KO expression (NSAF presence/absence) explained by bacterial species, environmental conditions and microbial community composition. Right: linear regression model depicting the contribution of each factor to KO variance. Statistical significance was assessed using ANOVA.

Functional overlap is reduced in microbial communities

We have examined the specific effects that individual microbial counterparts have on the protein abundance of single-species populations. We have also determined that proteomic changes in response to community composition and carbon source occur across diverse metabolic functions rather than being confined to particular pathways. We next asked whether the observed modulation in genome expression within community contexts corresponded to a decrease in functional overlap between community members. To assess the later hypothesis, we annotated the expressed genes in each culture using KO terms and compared the modulated genes across three levels of KEGG classification (L1, broad functional categories; L2, subcategories; and L3, specific pathways) as well as at the individual KO level. We then calculated the expected functional overlap (calculated as the combined functions of two single-species cultures or mixed isolates without considering genomic potential) with the observed overlap in pairwise communities or full consortia. Strikingly, in the vast majority of cases (83%), we observed a significant reduction in functional overlap (Fig. 5a,b, Extended Data Figs. 8 and 9, and Supplementary Figs. 1 and 2). This observation led us to hypothesize that the reduction in functional redundancy, potentially reflecting niche differentiation and reduced interspecies competition, may contribute to increased productivity (Fig. 5c). In this context, individual microbes may lower their protein production burden (a major energy cost[38]) while benefiting from metabolites or resources made available by neighbouring species. To test the potential link

https://doi.org/10.1038/s41564-026-02310-w

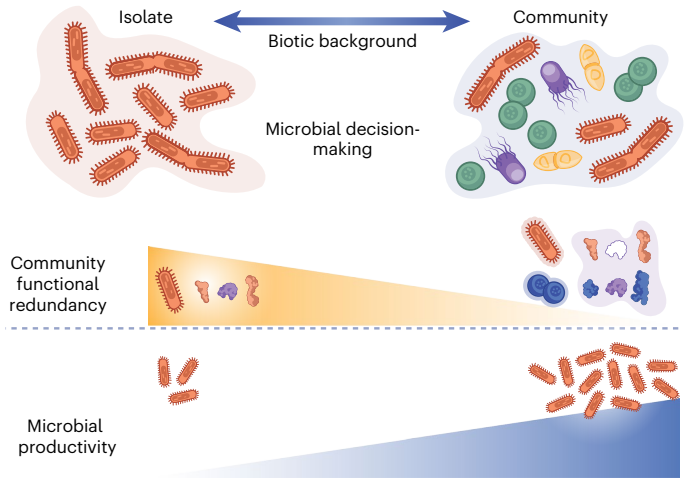

Fig. 6 | Schematic model of the findings revealed in our study. Our data provide molecular evidence that microbes actively modulate their realized niches in response to community composition, reducing functional overlap as a potential mechanism for niche partitioning (microbial decision-making), while enhancing community productivity. Altogether, these findings demonstrate a selective advantage for proteome-level plasticity and point to generalizable molecular mechanisms that support microbial coexistence.

between functional specialization and productivity gain, we quantified community productivity by comparing observed cell numbers with those expected from a theoretical additive model based on monoculture performance (see Methods). We found a statistically significant association between reduced functional overlap and increased community productivity (odds ratio (OR) = 9.75; Wald test one-sided $P = 0.038$; Fig. 5b). Of note, we did not detect a linear or monotonic (rank-based) relationship between functional overlap and productivity across the examined range, suggesting that additional interacting factors probably contribute to the observed productivity gains. These observations warrant further investigation into the mechanisms governing this relationship.

To better understand the general drivers of protein abundance reduction, we constructed a linear model to quantify the contributions of species identity, carbon source (abiotic factor) and microbial composition (biotic factor) to the observed variance in the number of expressed KOs. The model revealed that 24% of the variance between predicted and observed KO counts could be attributed to species identity, consistent with intrinsic regulatory differences across microbes. Biotic interactions, defined as the presence and identity of other community members, explained an additional 19% of the variance, while the abiotic factor (carbon source) contributed only 1.5%. Notably, the correlation between community composition and the number of expressed KOs was strong ($R = 0.67$), indicating a consistent directional trend towards protein abundance reduction that is primarily driven by biotic interactions when species identity is not considered. The full model explained 45.2% of the total variance when accounting for main effects and their interactions (Fig. 5d and Supplementary Fig. 3), and its explanatory power increased to 74.8% when biotic–abiotic interaction terms were included. These findings highlight that microbial interactions exert a strong, directional and reproducible influence on protein abundance, favouring a reduction in expressed functions in response to community context. This pattern is most clearly illustrated in a principal component analysis of the proteomes from the *M. elsdenii* and *F. prausnitzii* pair (Extended Data Fig. 10), where the two factors are distinctly separated: the majority of variance is captured along the first principal component, which reflects biotic interactions, while the second component accounts for more modest variance associated with abiotic factors. This serves as a striking example of how both biotic and abiotic forces shape microbial protein abundance in an integrated manner.

Finally, we examined reoccurring functions that were expected to overlap and were always reduced by at least one member of the community (reduced overlap) and recurring functions that were expected as overlapping but were always maintained by each member of the community (maintained overlap). We examined the corresponding KEGG modules (Supplementary Table 2) and observed that functions consistently reduced across the consortia were predominantly associated with pathways related to adaptation, specialization and secondary metabolism, processes often specific to particular organisms or environmental conditions. In contrast, functions that were consistently retained corresponded to core metabolic pathways critical for survival, including fundamental processes required for energy production and biomass precursor synthesis. These core pathways represent primary metabolism, which is essential for organismal viability and cannot be bypassed. Meanwhile, pathways involved in cofactor and vitamin biosynthesis, although essential for normal enzyme activity, were in some cases reduced or no longer expressed, reflecting their conditional essentiality depending on the organism's capacity to scavenge or import these compounds from the environment.

Discussion

Here we devised a stepwise experimental approach using synthetic microbial communities with distinct phylogenetic backgrounds to mimic gut environments, aiming to investigate how both biotic and abiotic factors influence microbial protein expression and productivity. Our results demonstrate that biotic context exerts a dominant influence: across species and conditions, variation in community composition explained significantly more of the proteomic response than changes in carbon source. This partner-specific modulation of protein abundance suggests that microbes respond not only to environmental conditions but also to the identity of coexisting species. These biotic-driven responses were almost consistently accompanied by a reduction in functional overlap (Fig. 6). While core metabolic pathways were maintained, accessory and specialized functions were downregulated, leading to reduced proteomic overlap across species. These changes were associated with community productivity benefits, implying that microbes may optimize energy allocation in community by minimizing costly, redundant expression (Fig. 6). Nevertheless, the absence of a monotonic relationship between reductions in functional redundancy during microbial species coexistence and productivity indicates that this association warrants further examination across broader datasets, environmental contexts and controlled experiments. Although we did not directly measure competition or coexistence, our results support the hypothesis that regulatory plasticity reduces functional overlap, potentially facilitating niche partitioning and cross-feeding. From an ecological perspective, microbes appear to modulate their realized niche, the subset of their fundamental metabolic potential that is expressed in a given context, in response to community composition. This capacity to dynamically adjust protein abundance in relation to specific partners enables functional flexibility and may underlie key principles of microbial coexistence. Importantly, we observed that this flexibility is not uniform across species. For example, on fibre *E. hallii* exhibited marked, partner-specific changes in protein expression, consistent with its known metabolic versatility[27]. In contrast, *F. prausnitzii* showed more stable expression profiles, possibly reflecting a more constrained ecological role. Such contrasts suggest that some microbes, particularly generalists, may flexibly reshape their functional roles depending on their partners, whereas specialists may retain fixed functional inputs and outputs. Over time, such patterns of division of labour may contribute to the emergence of auxotrophies in microbial ecosystems as a long-term consequence of functional redundancy reduction, whereby microbes evolve to rely on coexisting species for essential metabolites to persist and thrive[39,40].

The observed reduction in functional overlap also aligns with known energetic constraints: overexpression of unnecessary genes can reduce productivity[38,41,42], and protein synthesis is tightly regulated under nutrient-limited conditions[38,41,43]. Our findings extend these principles to community settings, demonstrating that microbes adjust their protein expression not only in response to abiotic constraints but also to the presence and identity of their neighbours, effectively engaging in context-dependent 'decision making' that enhances their metabolic efficiency. This supports emerging frameworks of collective metabolism, where microbial communities self-organize into cooperative configurations by distributing metabolic functions, as predicted by resource allocation models[44] and computationally formalized in recent metabolic frameworks[45]. In summary, our study provides experimental evidence that microbial communities exhibit consistent patterns of functional streamlining via partner-dependent protein abundance. This reduction in functional overlap probably contributes to community stability by enabling division of labour, niche partitioning and energetic efficiency[46–48]. These principles can help guide future efforts to understand, predict and engineer microbial ecosystems across various applications, including health, agriculture and the environment.

Methods

Bacterial cultures

The bacterial strains *P. ruminicola* ATCC 19189, *M. elsdenii* DSM 20460, *B. fibrisolvens* DSM 3071, *E. hallii* DSM 3353, *R. intestinalis* DSM 14610, *M. formatexigens* DSM 14469 and *F. prausnitzii* DSM 17677 were obtained from ATCC and DSMZ. Strains were cultivated as single cultures, in pairwise cultures and in full consortia which were combined by species typically found in the bovine rumen (*P. ruminicola*, *M. elsdenii*, *B. fibrisolvens*, *E. hallii*) and in the human gut (*E. hallii*, *R. intestinalis*, *M. formatexigens*, *F. prausnitzii*). Bacteria were grown anaerobically in Hungate tubes containing yeast casitone fatty acids (YCFA) medium[49], supplemented with 0.5% wheat straw fibre (collected at the Agricultural Research Organization, Volcani Center, Israel) or 0.5% fructose as carbon sources for 24 h at 37 °C. To ensure bacterial community stability, the cultures were transferred to fresh media every 24 h over a span of 5 transfers. Each of the selected species is capable of growing on both media independently but cannot grow on media that is depleted of a carbon source. Chemicals were ordered from Sigma-Aldrich. The cultivation media were filter sterilized and degassed overnight in an anaerobic chamber (COY Lab) with a gas composition of 75% nitrogen, 20% carbon dioxide and 5% hydrogen. A volume of 3 ml of YCFA media (2×) was injected into anaerobic Hungate tubes pre-autoclaved with 3 ml 0.5% fructose or fibre in deuterium-depleted water using a 0.22 µm filter (Merck Millipore). Single, pairwise and full consortia cultures were obtained by inoculation of 100 µl of overnight cultures of the respective bacteria diluted in sterile saline solution to optical density (OD) 0.3. Biological triplicate cultures were performed for each experiment. To distinguish true biological reductions in functional redundancy from potential quantification artefacts, our experimental design included a dedicated control that mirrors the consortia but lacks biological interactions. Specifically, we generated mixed isolates by physically mixing protein extracts of the single species consortia based on summed normalized spectral abundance factor (NSAF) percentages (Supplementary Table 3) observed in the naturally assembled consortium. This produces an artificial community in which all species contribute their monoculture proteomes at the correct ratios. Because both the mixed isolates and the true consortia contain the full complement of species, KO identification and quantification depend solely on expression differences, allowing us to isolate biological effects of co-culturing from technical or compositional biases.

Quantitative PCR

Quantitative PCR served to determine the copy number of each bacterial strain in all cultures. The pellets of 1 ml cultures were obtained by centrifugation for 5 min at 4,000 *g*, and the genomic DNA was extracted by resuspending the pellets in 100 µl Tris-EDTA buffer, boiling them for 15 min at 95 °C and incubating them on ice for 15 min. The samples were then centrifuged for 5 min at 10,000 *g*. A volume of 2 µl of the supernatants (10-fold dilution) was used in a 10 µl reaction mix containing 5 µl absolute blue SYBR green master mix (Thermo Scientific) and 0.5 µl of each primer (at 10 mM).

Standard curves suitable for the quantification of each strain's 16S rRNA gene were generated by amplifying serial 10-fold dilutions of quantified gel-extracted PCR products, obtained by amplification of each fragment (primers in Supplementary Table 4), and were calculated using the Rotorgene 6000 series software (Qiagen). Real-time PCR was performed in a 10 µl reaction mixture.

Microbes that represented less than 5% of the relative abundance were excluded from the analyses, as they consistently had fewer than 400 detected proteins per genome across all tested conditions. Hence, individual microbial proteomes were included in subsequent analyses only when a minimum of 400 proteins were detected per bacterium, ensuring reliable proteomic measurements and enabling comparable analyses. The productivity of microbial communities was calculated as the ratio of total microbial abundance measured by qPCR in consortia to the mean microbial abundance of each isolate in monocultures (productivity = microbial abundance of consortia / $\bar{x}$ microbial abundance of isolates).

Proteomic samples preparation

To improve proteomic coverage, cell pellets and supernatants were processed separately for all cultivation types (single, pairwise and consortia). The cell pellet and supernatant from a 5 ml culture were collected and fractionated via centrifugation (5,000 *g*, 10 min, 4 °C) and stored at −80 °C until further preparation. All cell pellets were resuspended in 100 µl lysis buffer (8 M urea/2 M thiourea) and cells were disrupted using ultrasonication in a microtube holder with a BR-30 probe (Bandelin) for 5 cycles (1 min each at full amplitude). After centrifugation (15,000 *g*, 30 min, 4 °C), protein concentrations were determined using the Bradford assay[50].

For single cultures, 4-species consortia and mixed isolates. Protein cell extract (20 µg) was mixed with 5× reducing Laemmli buffer (250 mM Tris-HCl pH 6.8, 50% glycerol, 10% SDS, 37.5 µl ml^{-1} ß-mercaptoethanol) and incubated at 95 °C for 5 min before loading onto precast gels for electrophoretic separation. Electrophoretic separation was performed via SDS–PAGE with 4–20% Criterion TGX Precast Midi Protein Gel (BIO-RAD) for 5–15 min at 25 V, followed by 35–45 min at 180 V. If the sample volume had exceeded 35 µl, the sample was divided into two loading pockets.

After Coomassie staining, each lane was processed as previously described[51]. Briefly, each gel lane was cut into 10 pieces and further into small 2 × 2 mm cubes. If a sample had been split into two lanes, gel pieces were pooled before digestion. The gel pieces were destained at least two times in 700 µl washing solution (200 mM ammonium bicarbonate (ABC), 30% acetonitrile (ACN)) for 15 min at 37 °C (900 r.p.m.) before being dehydrated with 500 µl ACN and dried completely. For protein digestion, 120 µl of trypsin solution (2 µg ml^{-1}, Promega) was added and excess trypsin solution was removed after a short incubation. Digestion was performed in a Thermomixer (Eppendorf) at 37 °C for 14 h at 1,000 r.p.m. Peptides were eluted in 80 µl ASTM type 1 water in a sonication bath for 15 min (Sonorex Super RK 102 H, Bandelin), dried and resuspended in 10 µl solvent A (0.1% acetic acid in ASTM type 1 water) containing 1× Biognosys iRT standard (Biognosys) before storage at −20 °C.

Protein cell extracts of pairwise cultivation pellets were processed using S-Trap micro spin columns (Protifi), followed by basic pH reversed-phase fractionation according to manufacturer instructions, with some modifications. Briefly, 20 µg of protein was mixed with

2× SDS lysis buffer (10% SDS, 100 mM triethylammonium bicarbonate (TEAB) pH 7.55) incubated in the ultrasonication bath before reduction (100 mM in 50 mM TEAB; 10 min, 95 °C) and alkylation (50 mM TEAB for 30 min at 20 °C in the dark) were performed. Samples were acidified and diluted in S-Trap binding buffer (90% methanol, 100 mM TEAB pH 7.1). Sample mixtures were applied to the S-Trap column, washed twice and digested with 25 µl of 1:25 trypsin solution (prepared from 1:10 trypsin stock in 50 mM TEAB) for 3 h at 47 °C. Peptides were eluted in three steps with: 40 µl 50 mM TEAB, 40 µl 0.1% acetic acid and 35 µl 60% ACN in 0.1% acetic acid before eluates were pooled and dried completely. Peptides were eluted subsequently with 300 µl of elution solutions with an increasing ACN gradient in 0.1% triethylamine solution. Fractions were collected separately, pooled orthogonally, dried in a vacuum centrifuge and resuspended in 20 µl solvent A containing 0.1× Biognosys iRT standard before storage at −20 °C.

Supernatant fractions of single cultures, 4-species consortia and mixed-isolates consortia were enriched with StrataClean beads[51] (Agilent). Briefly, pre-hydrolysed StrataClean beads were mixed with 200 µl–1 ml of sample supernatant and incubated overnight at 4 °C (Multi-Rotator PTR-35, Grant-Bio). After centrifugation (10,000 *g*, 45 min, 4 °C), the StrataClean bead pellets were washed in 1 ml ASTM type 1 water, dried in a vacuum centrifuge, resuspended in 30 µl 2× reducing Laemmli sample buffer and incubated (10 min, 98 °C) before loading onto precast gels for electrophoretic separation. Afterwards, the samples were in-gel digested as described above and resuspended in 10 µl solvent A containing 1× Biognosys iRT standard before storage at −20 °C. The gel pieces of the pairwise consortia supernatants were destained as described above before additional reduction (100 µl 10 mM dithiothreitol in 25 mM ABC for 1 h at 56 °C) and alkylation (100 µl 55 mM iodoacetamide for 45 min at 20 °C in the dark) was performed. The samples were processed as described above and resuspended in 11 µl solvent A containing 0.1× Biognosys iRT standard before storage at −20 °C.

LC–MS/MS measurement and data analysis. Peptides were separated on different LC systems equipped with in-house packed 20 cm reversed-phase columns (100 µm inner diameter, 360 µm outer diameter) filled with ReproSil-Pur 120 C18-AQ resin (3 µm particle size, Dr Maisch) and injected into different Orbitrap-based mass spectrometers (Thermo Fisher). All instruments and settings used are listed in Supplementary Table 5. Databases included predicted open reading frames (ORFs) (using Prokka[52]) of the respective bacteria inoculated in the samples, common laboratory contaminants and the wheat fibre used as one carbon source in this study. One database contained predicted ORFs of species typically found in consortium 1 (*P. ruminicola*, *M. elsdenii*, *B. fibrisolvens, E. hallii*) and another of species typical of consortium 2 (*E. hallii*, *R. intestinalis*, *M. formatexigens*, *F. prausnitzii*). Databases were filtered for sequence duplicates using seqkit[53] and concatenated to reverse entries for each protein. Applied databases were deposited in PRIDE (see Data availability statement).

For NSAF quantifications used to prepare the mixed isolates, the MS *.raw files were searched against the sample-specific databases using Mascot[54] (v.2.7.0.1) with the following parameters: precursor mass tolerance ±10 ppm; fragment mass tolerance ±0.5 Da; tryptic digestion with up to two missed cleavages; searching monoisotopic mass values only; only consider charge states 2+, 3+ and 4+; variable modification: methionine oxidation (+16 Da), fixed modification (pairwise cultures only): cysteine carbamidomethylation (+57 Da). Resulting *.dat files were loaded into Scaffold[55] (v.5.0.1) with the databases used for Mascot searches, and an additional X!Tandem[56] (v.2017.2.1.2) search was performed with default settings. Peptide identifications were accepted if they could be established at greater than 95.0% probability by the 'peptide prophet' algorithm[57] with Scaffold delta-mass correction. Protein identifications were accepted if they could be established at greater than 99.0% probability and contained at least 2 identified unique peptides. Protein probabilities were assigned by the 'protein prophet' algorithm[57]. Proteins that contained shared peptides and could not be differentiated based on MS/MS analysis alone were grouped to satisfy the principles of parsimony.

For label-free quantification (LFQ), MS *.raw files were analysed using FragPipe (v.23.0)[58] by searching against the databases described above. Search parameters of MSFragger (v.4.3)[59,60] were set as follows: precursor mass tolerance −20 to 20 PPM; fragment mass tolerance 0.2 Da; strict trypsin digestion (cuts KR) with maximal two missed cleavages; maximum of three variable modifications including oxidation M (+15.9949) and N-terminal acetylation (+42.0106); and fixed modification cysteine carbamidomethylation (+57.02146) for the pairwise cultivation samples. Peptide-spectrum matches (PSMs), peptides and proteins were validated and filtered at 1% false-discovery rate (FDR) using MSBooster[61] and Percolator[62] in tandem with Philosopher (v.5.1.1)[63]. Protein abundances were quantified using IonQuant (v.1.11.11)[64] based on MaxLFQ values (minimum two ions per protein, 1% FDR for match-between-runs, utilizing only unique peptides for protein quantification based on a strict peptide-protein uniqueness setting, no normalization across runs). For functional overlap analysis, MaxLFQ values were based on unique and shared peptides. All MaxLFQ values were median normalized on the basis of iRT signals[65] and resulting LFQ values were $\log_2$ transformed.

In general, a protein was only considered as identified if at least two unique peptides were identified. All proteins identified and quantified, together with their quantitative values, numbers of unique peptides and unique spectral counts are provided in the Supplementary Tables 6 and 7. Across species, we identified on average more than 1,000 proteins per genome, and ~1,600 proteins per run (Supplementary Fig. 4). This corresponds to ~40% genome coverage—approximately 70% of the expressed and mass-spectrometry-accessible proteome—and is well within the range of accepted high-quality bacterial proteomics workflows[66].

PCA and principal coordinates analysis (PCoA)

PCA was performed using LFQ values of all genes from either supernatant (secreted proteins) or pellet fractions (cytosolic proteins); if the two carbon sources were plotted on the same plot together with the two fractions, the effect of the fractions was corrected using the 'Combat' function of the 'sva' R package[67]. Missing values were imputed on the basis of the probabilistic minimum method (MinProb function in the LCMD package[68]). PCoA was performed using presence/absence data of identified proteins from both the supernatant and pellet fractions. The analysis was conducted with the phyloseq R package[69] to assess overall proteomic variation across different species, carbon sources and community compositions. Dissimilarity matrices were calculated using either Bray–Curtis or Jaccard indexes (PCA or PCoA, respectively). Clustering patterns were visualized on both PCA and PCoA plots, the statistical significance of group separation was evaluated using ANOSIM as implemented in the vegan R package[70] with 10,000 permutations, and *P* values were corrected using FDR Benjamini–Hochberg correction. Plots were generated using the ggplot2 R package[71].

Functional redundancy analysis

Proteomic profiles for each bacterial strain were annotated using the KEGG database[72]. Identified proteins per genome, quantified with at least two unique peptides and assignable to a single species and in at least one fraction (cytosolic or secreted proteins), were mapped to KO identifiers and further classified into functional pathways across KEGG BRITE levels 1 (broad functional categories), 2 (subcategories) and 3 (specific metabolic pathways). In this presence/absence analyses performed for functional redundancy interpretation, all peptides, including shared peptides, were used, and protein identification was performed by Mascot in combination with X!Tandem searches. Only KOs associated with KEGG pathway map01100 (metabolic pathways) were considered. Heat maps were generated using the pheatmap

R package. Functional overlap was calculated as the relative difference between the number of distinct KOs observed in a community and the total number of distinct KOs expected based on the sum of those identified in the corresponding monocultures, using the formula:

$$\text{Functional Overlap}\,(\%) = \left(\text{Observed Overlap}_{\text{community}} - \text{Expected Overlap}_{\text{monocultures}}\right) \div \text{Observed Overlap}_{\text{community}} \times 100 \quad (1)$$

To investigate functional overlap within the microbial consortia, we focused on recurring KOs that were expected to be shared among community members. We categorized these functions into two groups: those that were consistently reduced, meaning they were expected to overlap but were absent or lost in at least one community member (reduced overlap), and those that were consistently maintained, meaning they were expected to overlap and were present in every member of the community (maintained overlap). Recurring functions were defined as KOs found in at least 10 different bacterial communities. To characterize the metabolic pathways associated with these KOs, we mapped each KO to its corresponding KEGG modules by querying the KEGG REST API[73].

A linear regression model was implemented in R using the lm() function to assess the relationship between the total number of distinct KOs and explanatory variables such as bacterial species, environmental conditions and microbial community composition. The variance in KO expression attributable to each factor was evaluated using analysis of variance (ANOVA).

Reporting summary

Further information on research design is available in the Nature Portfolio Reporting Summary linked to this article.

Data availability

The mass spectrometry proteomics data have been deposited in the ProteomeXchange Consortium via the PRIDE partner repository[74] with the dataset identifiers PXD071838, PXD072222 and PXD073583. Source data are provided with this paper.

References

1. Hou, K. et al. Microbiota in health and diseases. *Signal Transduct. Target. Ther.* **7**, 135 (2022).
2. Arrigo, K. R. Marine microorganisms and global nutrient cycles. *Nature* **437**, 349–355 (2005).
3. Hartmann, M. & Six, J. Soil structure and microbiome functions in agroecosystems. *Nat. Rev. Earth Environ.* **4**, 4–18 (2022).
4. Tilman, D. *Resource Competition and Community Structure* (Princeton Univ. Press, 1982).
5. Thébault, E. & Fontaine, C. Stability of ecological communities and the architecture of mutualistic and trophic networks. *Science* **329**, 853–856 (2010).
6. Baran, R. et al. Exometabolite niche partitioning among sympatric soil bacteria. *Nat. Commun.* **6**, 8289 (2015).
7. Strachan, C. R. et al. Differential carbon utilization enables co-existence of recently speciated Campylobacteraceae in the cow rumen epithelial microbiome. *Nat. Microbiol.* **8**, 309–320 (2023).
8. Peng, X. et al. Metabolic interdependencies in thermophilic communities are revealed using co-occurrence and complementarity networks. *Nat. Commun.* **15**, 8166 (2024).
9. Blanchard, A. E. & Lu, T. Bacterial social interactions drive the emergence of differential spatial colony structures. *BMC Syst. Biol.* **9**, 59 (2015).
10. Moraïs, S. et al. Plasmid-encoded toxin defence mediates mutualistic microbial interactions. *Nat. Microbiol.* **9**, 108–119 (2024).
11. Shade, A. et al. Fundamentals of microbial community resistance and resilience. *Front. Microbiol.* **3**, 417 (2012).
12. Wang, W. et al. Narrow-spectrum resource-utilizing bacteria drive the stability of synthetic communities through enhancing metabolic interactions. *Nat. Commun.* **16**, 6088 (2025).
13. Phelan, V. V., Liu, W.-T., Pogliano, K. & Dorrestein, P. C. Microbial metabolic exchange—the chemotype-to-phenotype link. *Nat. Chem. Biol.* **8**, 26–35 (2011).
14. Moreno-Gámez, S., Hochberg, M. E. & van Doorn, G. S. Quorum sensing as a mechanism to harness the wisdom of the crowds. *Nat. Commun.* **14**, 3415 (2023).
15. Hibbing, M. E., Fuqua, C., Parsek, M. R. & Peterson, S. B. Bacterial competition: surviving and thriving in the microbial jungle. *Nat. Rev. Microbiol.* **8**, 15–25 (2010).
16. Goldford, J. E. et al. Emergent simplicity in microbial community assembly. *Science* **361**, 469–474 (2018).
17. Hutchinson, G. E. The paradox of the plankton. *Am. Nat.* **95**, 37–145 (1961).
18. Mascher, T., Helmann, J. D. & Unden, G. Stimulus perception in bacterial signal-transducing histidine kinases. *Microbiol. Mol. Biol. Rev.* **70**, 910–938 (2006).
19. Jacob, F. & Monod, J. Genetic regulatory mechanisms in the synthesis of proteins. *J. Mol. Biol.* **3**, 318–356 (1961).
20. Hutchinson, G. E. Concluding remarks. *Cold Spring Harb. Symp. Quant. Biol.* **22**, 415–427 (1957).
21. Dekel, E. & Alon, U. Optimality and evolutionary tuning of the expression level of a protein. *Nature* **436**, 588–592 (2005).
22. Scott, M., Gunderson, C. W., Mateescu, E. M., Zhang, Z. & Hwa, T. Interdependence of cell growth and gene expression: origins and consequences. *Science* **330**, 1099–1102 (2010).
23. Flamholz, A., Noor, E., Bar-Even, A., Liebermeister, W. & Milo, R. Glycolytic strategy as a tradeoff between energy yield and protein cost. *Proc. Natl Acad. Sci. USA* **110**, 10039–10044 (2013).
24. Sasson, G. et al. Metaproteome plasticity sheds light on the ecology of the rumen microbiome and its connection to host traits. *ISME J.* **16**, 2610–2621 (2022).
25. Weiss, A. S. et al. In vitro interaction network of a synthetic gut bacterial community. *ISME J.* **16**, 1095–1109 (2022).
26. Mizrahi, I., Wallace, R. J. & Moraïs, S. The rumen microbiome: balancing food security and environmental impacts. *Nat. Rev. Microbiol.* **19**, 553–566 (2021).
27. Duncan, S. H., Louis, P. & Flint, H. J. Lactate-utilizing bacteria, isolated from human feces, that produce butyrate as a major fermentation product. *Appl. Environ. Microbiol.* **70**, 5810–5817 (2004).
28. Duncan, S. H. *Roseburia intestinalis* sp. nov., a novel saccharolytic, butyrate-producing bacterium from human faeces. *Int. J. Syst. Evol. Microbiol.* **52**, 1615–1620 (2002).
29. Wolin, M. J., Miller, T. L., Collins, M. D. & Lawson, P. A. Formate-dependent growth and homoacetogenic fermentation by a bacterium from human feces: description of *Bryantella formatexigens* gen. nov., sp. nov. *Appl. Environ. Microbiol.* **69**, 6321–6326 (2003).
30. Parsaei, M., Sarafraz, N., Moaddab, S. Y. & Ebrahimzadeh Leylabadlo, H. The importance of *Faecalibacterium prausnitzii* in human health and diseases. *New Microbes New Infect.* **43**, 100928 (2021).
31. Betancur-Murillo, C. L., Aguilar-Marín, S. B. & Jovel, J. *Prevotella*: a key player in ruminal metabolism. *Microorganisms* **11**, 1 (2022).
32. Brown, D. W. & Moore, W. E. C. Distribution of *Butyrivibrio fibrisolvens* in nature. *J. Dairy Sci.* **43**, 1570–1574 (1960).
33. da Silva Cabral, L. & Weimer, P. J. *Megasphaera elsdenii*: its role in ruminant nutrition and its potential industrial application for organic acid biosynthesis. *Microorganisms* **12**, 219 (2024).

34. Yoav, S. et al. How does cellulosome composition influence deconstruction of lignocellulosic substrates in *Clostridium*(*Ruminiclostridium*) *thermocellum* DSM 1313? *Biotechnol. Biofuels* **10**, 222 (2017).
35. Esser, D. et al. Change of carbon source causes dramatic effects in the phospho-proteome of the archaeon *Sulfolobus solfataricus*. *J. Proteome Res.* **11**, 4823–4833 (2012).
36. Zhivin-Nissan, O. et al. Unraveling essential cellulosomal components of the (*Pseudo*)*Bacteroides cellulosolvens* reveals an extensive reservoir of novel catalytic enzymes. *Biotechnol. Biofuels* **12**, 115 (2019).
37. Artzi, L., Morag, E., Barak, Y., Lamed, R. & Bayer, E. A. *Clostridium clariflavum*: key cellulosome players are revealed by proteomic analysis. *MBio* **6**, e00411-15 (2015).
38. Shachrai, I., Zaslaver, A., Alon, U. & Dekel, E. Cost of unneeded proteins in *E. coli* is reduced after several generations in exponential growth. *Mol. Cell* **38**, 758–767 (2010.
39. Morris, J. J., Lenski, R. E. & Zinser, E. R. The Black Queen Hypothesis: evolution of dependencies through adaptive gene loss. *MBio* **3**, e00036-12 (2012).
40. Tovar-Herrera, O. E. et al. Core rumen microbes are functional generalists that sustain host metabolism and gut ecosystem function. *Nat. Ecol. Evol.* **10**, 44–58 (2026).
41. You, C. et al. Coordination of bacterial proteome with metabolism by cyclic AMP signalling. *Nature* **500**, 301–306 (2013).
42. Dong, H., Nilsson, L. & Kurland, C. G. Gratuitous overexpression of genes in *Escherichia coli* leads to growth inhibition and ribosome destruction. *J. Bacteriol.* **177**, 1497–1504 (1995).
43. Merchant, S. S. & Helmann, J. D. Elemental economy: microbial strategies for optimizing growth in the face of nutrient limitation. *Adv. Microb. Physiol.* **60**, 91–210 (2012).
44. Kim, M., Sung, J. & Chia, N. Resource-allocation constraint governs structure and function of microbial communities in metabolic modeling. *Metab. Eng.* **70**, 12–22 (2022).
45. Huelsmann, M., Schubert, O. T. & Ackermann, M. A framework for understanding collective microbiome metabolism. *Nat. Microbiol.* **9**, 3097–3109 (2024).
46. D'Souza, G. et al. Ecology and evolution of metabolic cross-feeding interactions in bacteria. *Nat. Prod. Rep.* **35**, 455–488 (2018).
47. Embree, M., Liu, J. K., Al-Bassam, M. M. & Zengler, K. Networks of energetic and metabolic interactions define dynamics in microbial communities. *Proc. Natl Acad. Sci. USA* **112**, 15450–15455 (2015).
48. Tsoi, R. et al. Metabolic division of labor in microbial systems. *Proc. Natl Acad. Sci. USA* **115**, 2526–2531 (2018).
49. Lopez-Siles, M. et al. Cultured representatives of two major phylogroups of human colonic *Faecalibacterium prausnitzii* can utilize pectin, uronic acids, and host-derived substrates for growth. *Appl. Environ. Microbiol.* **78**, 420–428 (2012).
50. Bradford, M. A rapid and sensitive method for the quantitation of microgram quantities of protein utilizing the principle of protein-dye binding. *Anal. Biochem.* **72**, 248–254 (1976).
51. Bonn, F. et al. Picking vanished proteins from the void: how to collect and ship/share extremely dilute proteins in a reproducible and highly efficient manner. *Anal. Chem.* **86**, 7421–7427 (2014).
52. Seemann, T. Prokka: rapid prokaryotic genome annotation. *Bioinformatics* **30**, 2068–2069 (2014).
53. Shen, W., Le, S., Li, Y. & Hu, F. SeqKit: a cross-platform and ultrafast toolkit for FASTA/Q file manipulation. *PLoS ONE* **11**, e0163962 (2016).
54. Perkins, D. N., Pappin, D. J., Creasy, D. M. & Cottrell, J. S. Probability-based protein identification by searching sequence databases using mass spectrometry data. *Electrophoresis* **20**, 3551–3567 (1999).
55. Searle, B. C. Scaffold: a bioinformatic tool for validating MS/MS-based proteomic studies. *Proteomics* **10**, 1265–1269 (2010).
56. Craig, R. & Beavis, R. C. TANDEM: matching proteins with tandem mass spectra. *Bioinformatics* **20**, 1466–1467 (2004).
57. Keller, A., Nesvizhskii, A. I., Kolker, E. & Aebersold, R. Empirical statistical model to estimate the accuracy of peptide identifications made by MS/MS and database search. *Anal. Chem.* **74**, 5383–5392 (2002).
58. Nesvizhskii, A. I., Keller, A., Kolker, E. & Aebersold, R. A statistical model for identifying proteins by tandem mass spectrometry. *Anal. Chem.* **75**, 4646–4658 (2003).
59. Yu, F. et al. Fast quantitative analysis of timsTOF PASEF data with MSFragger and IonQuant. *Mol. Cell. Proteomics* **19**, 1575–1585 (2020).
60. Kong, A. T., Leprevost, F. V., Avtonomov, D. M., Mellacheruvu, D. & Nesvizhskii, A. I. MSFragger: ultrafast and comprehensive peptide identification in mass spectrometry-based proteomics. *Nat. Methods* **14**, 513–520 (2017).
61. Yang, K. L. et al. MSBooster: improving peptide identification rates using deep learning-based features. *Nat. Commun.* **14**, 4539 (2023).
62. The, M., MacCoss, M. J., Noble, W. S. & Käll, L. Fast and accurate protein false discovery rates on large-scale proteomics data sets with percolator 3.0. *J. Am. Soc. Mass. Spectrom.* **27**, 1719–1727 (2016).
63. da Veiga Leprevost, F. et al. Philosopher: a versatile toolkit for shotgun proteomics data analysis. *Nat. Methods* **17**, 869–870 (2020).
64. Yu, F., Haynes, S. E. & Nesvizhskii, A. I. IonQuant enables accurate and sensitive label-free quantification with FDR-controlled match-between-runs. *Mol. Cell. Proteomics* **20**, 100077 (2021).
65. Escher, C. et al. Using iRT, a normalized retention time for more targeted measurement of peptides. *Proteomics* **12**, 1111–1121 (2012).
66. Abele, M. et al. Unified workflow for the rapid and in-depth characterization of bacterial proteomes. *Mol. Cell. Proteomics* **22**, 100612 (2023).
67. Leek, J. T., Johnson, W. E., Parker, H. S., Jaffe, A. E. & Storey, J. D. The sva package for removing batch effects and other unwanted variation in high-throughput experiments. *Bioinformatics* **28**, 882–883 (2012).
68. Lazar, C., Gatto, L., Ferro, M., Bruley, C. & Burger, T. Accounting for the multiple natures of missing values in label-free quantitative proteomics data sets to compare imputation strategies. *J. Proteome Res.* **15**, 1116–1125 (2016).
69. McMurdie, P. J. & Holmes, S. phyloseq: an R package for reproducible interactive analysis and graphics of microbiome census data. *PLoS ONE* **8**, e61217 (2013).
70. Oksanen, J. et al. vegan: community ecology package. R package version 2.5-7 (2020).
71. Wickham, H. *ggplot2: Elegant Graphics for Data Analysis* (Springer, 2016).
72. Aramaki, T. et al. KofamKOALA: KEGG Ortholog assignment based on profile HMM and adaptive score threshold. *Bioinformatics* **36**, 2251–2252 (2020).
73. Kanehisa, M. & Goto, S. KEGG: Kyoto encyclopedia of genes and genomes. *Nucleic Acids Res.* **28**, 27–30 (2000).
74. Perez-Riverol, Y. et al. The PRIDE database resources in 2022: a hub for mass spectrometry-based proteomics evidences. *Nucleic Acids Res.* **50**, D543–D552 (2022).

Acknowledgements

This work was funded by grants from the European Research Council (ERC 866530), the Israel Science Foundation–Swiss National Science Foundation (ISF–SNSF 1057/24) and the Israel Science Foundation (979/25) to I.M. We thank L. Franzmeyer, J. Bosch and M. Toschke for proteomic sample preparations; S. Grund, T. Kroniger and C. Wünsche for proteomics measurements; J. Bartel for proteomics data analysis; and scientific artist D. Perlman for the scientific illustrations and assistance with graphic design in all figures of this paper.

Author contributions

I.M. and S. Moraïs designed research. S. Moraïs, M.M., I.A., I.G. and Y.S. performed research. P.G., A.T.-S., S. Maaß and D.B. performed proteomic analyses. I.M., S. Moraïs, M.M. and L.L. analysed data. S. Moraïs and. I.M. wrote the paper. I.M. secured funding.

Competing interests

The authors declare no competing interest.

Additional information

Extended data is available for this paper at https://doi.org/10.1038/s41564-026-02310-w.

Supplementary information The online version contains supplementary material available at https://doi.org/10.1038/s41564-026-02310-w.

Correspondence and requests for materials should be addressed to Itzhak Mizrahi.

Peer review information *Nature Microbiology* thanks Leyuan Li and the other, anonymous, reviewer(s) for their contribution to the peer review of this work.

https://doi.org/10.1038/s41564-026-02310-w

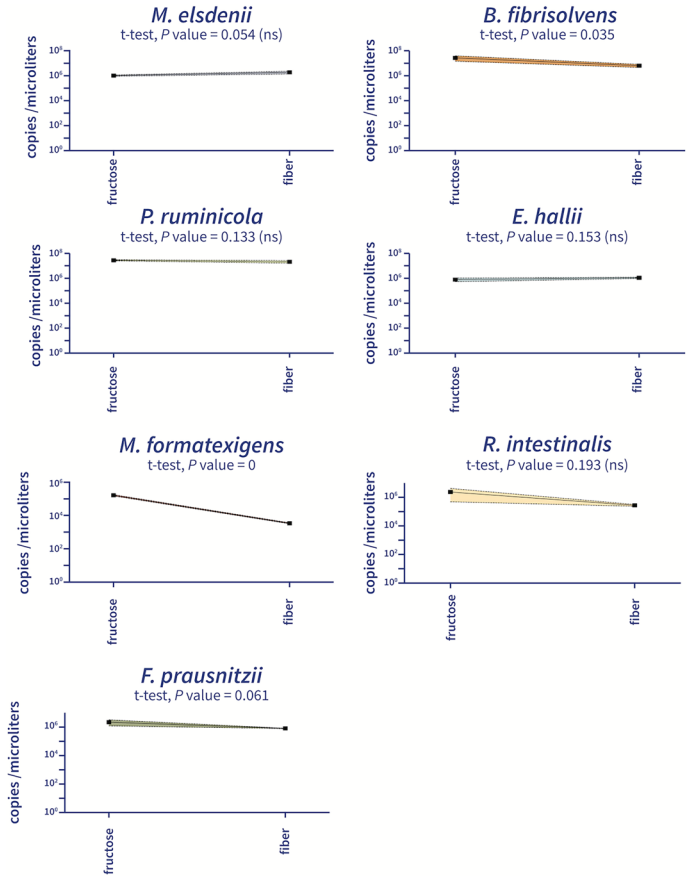

Extended Data Fig. 1 | Growth of individual bacteria on the two selected carbon sources. The growth of each microbial species in fructose or fiber as carbon source (n=3 biological replicates) is indicated by their concentration as determined by qPCR using specific primers in copies/microliters. Statistical significance between conditions was assessed using a two-sided t-test performed on log10-transformed values, with the corresponding *P* values indicated in each panel.

https://doi.org/10.1038/s41564-026-02310-w

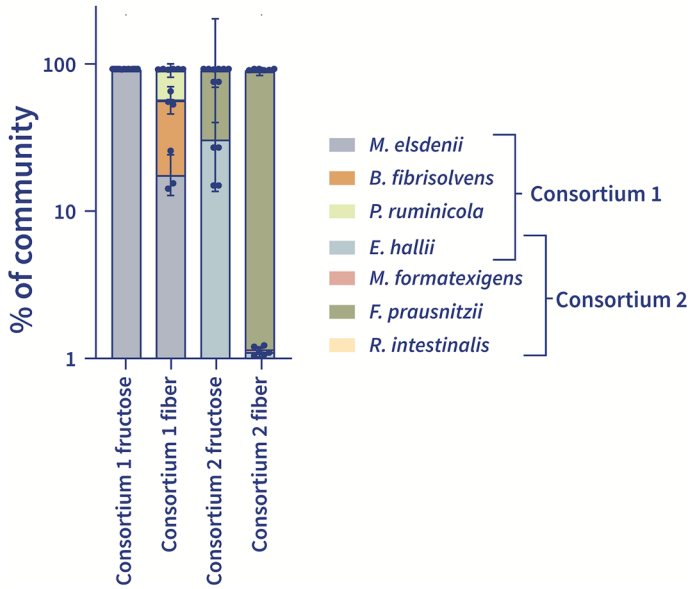

Extended Data Fig. 2 | Community structure of the assembled consortia. Bar plots depicting the microbial composition of each consortium, expressed as a percentage, as determined by qPCR using species-specific primers for each bacterial strain in 3 independent biological replicates.

https://doi.org/10.1038/s41564-026-02310-w

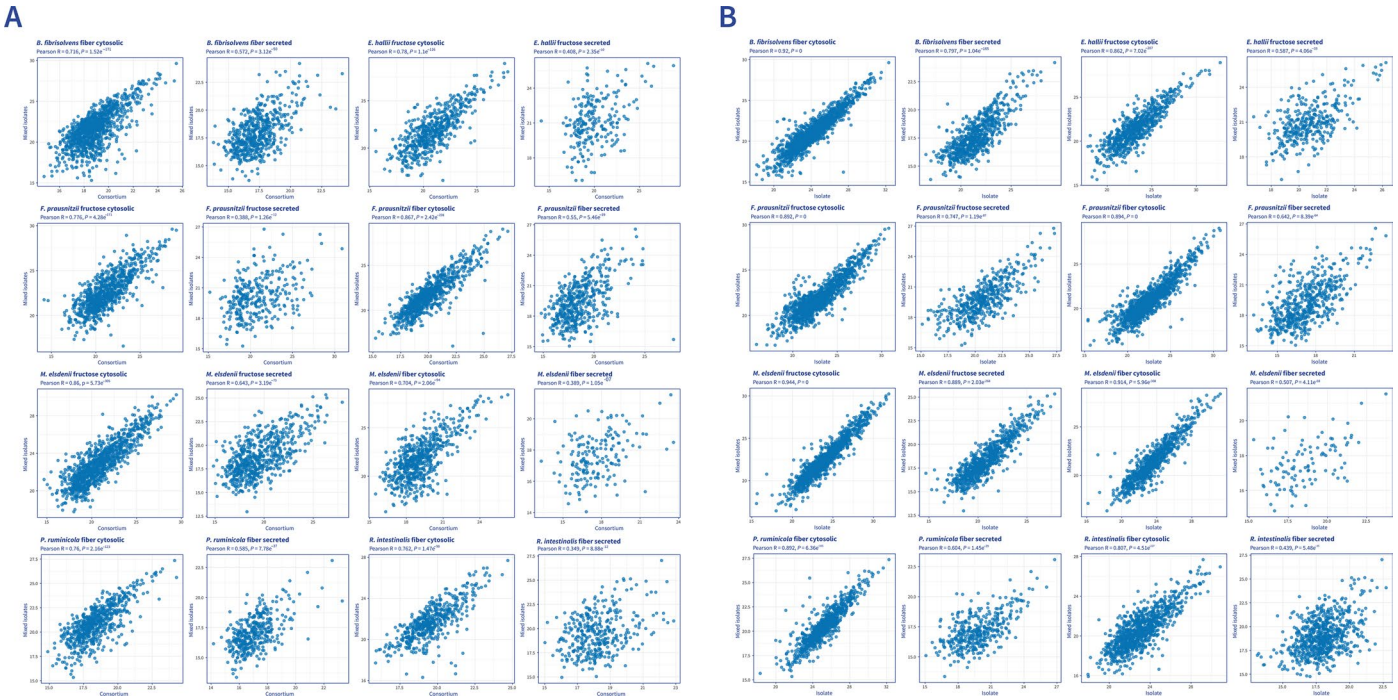

Extended Data Fig. 3 | Scatter plots of species-specific protein abundances, comparing the mixed isolates to the corresponding single-species cultures (A) or mixed isolates to the corresponding consortium (B). Each point represents a protein, with the x-axis showing the mean abundance (in 3 independent biological replicates) in the single-species cultures and the y-axis showing the mean abundance in the mixed isolates. Proteins present in both datasets are included, and the diagonal indicates perfect correlation. Across 15 out of 16 species, strong linear relationships are observed, Pearson correlation coefficients (two-sided) are given in Supplementary Table 1 and indicate that the proteomic profiles of individual species are largely preserved in the mixed isolates and more closely resemble those of the corresponding single-species cultures.

https://doi.org/10.1038/s41564-026-02310-w

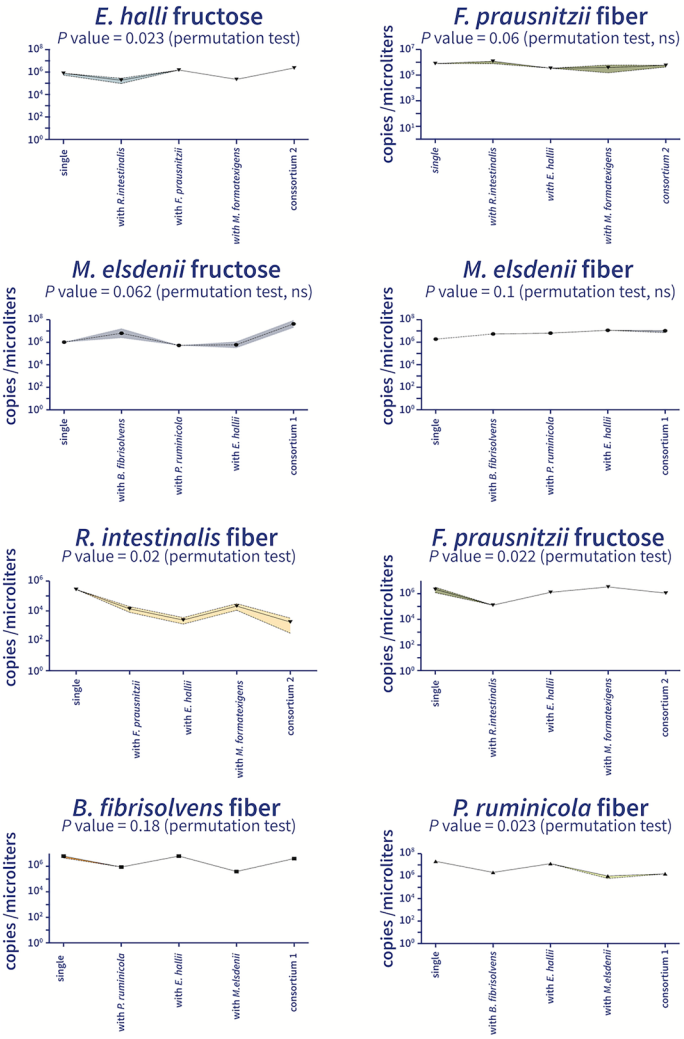

Extended Data Fig. 4 | Growth of bacteria as individuals or in varying community compositions. The growth of each microbial species (n=3 biological replicates) is indicated by its concentration as determined by qPCR using specific primers in copies/microliters. Statistical significance between conditions was assessed using a permutation test on the median, and the corresponding *P* values for two-sided permutation tests are indicated in each panel.

https://doi.org/10.1038/s41564-026-02310-w

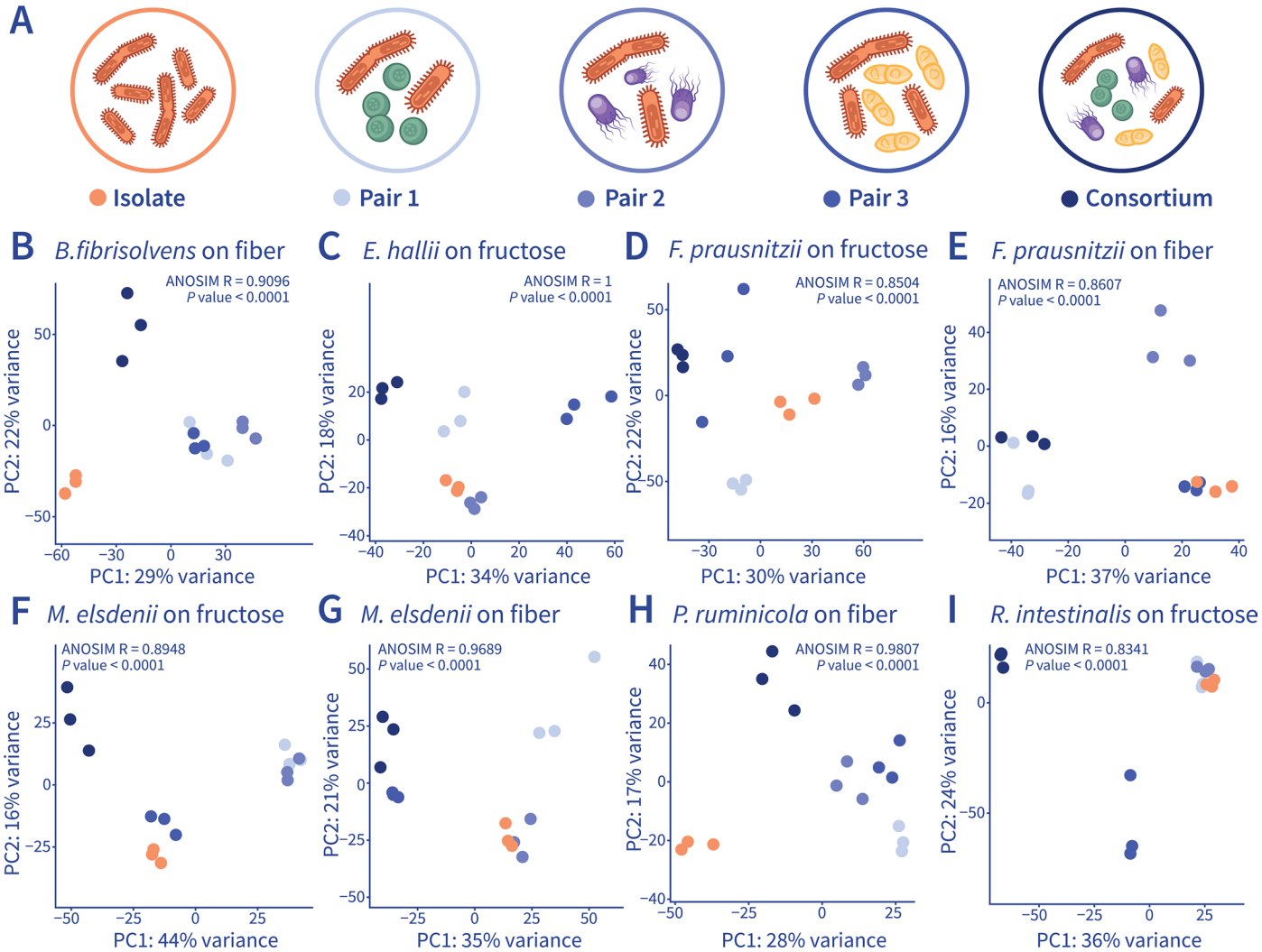

Extended Data Fig. 5 | Species-level proteomic responses are shaped by community context. a. Species-level proteomics were analysed for individual species, three different pairs and the consortia of four bacterial species. **b-i**. PCA of the overall proteomes (secreted proteins) for each of the indicated bacteria (LFQ values) and carbon source in the communities described in A (three biological replicates) (with corresponding color coding). Clustering analysis of expressed proteins according to the type of culture was performed using the ANOSIM test (two-sided) with 10000 randomizations of the data and the resulting R and *P* values corrected using FDR Benjamini–Hochberg are indicated.

https://doi.org/10.1038/s41564-026-02310-w

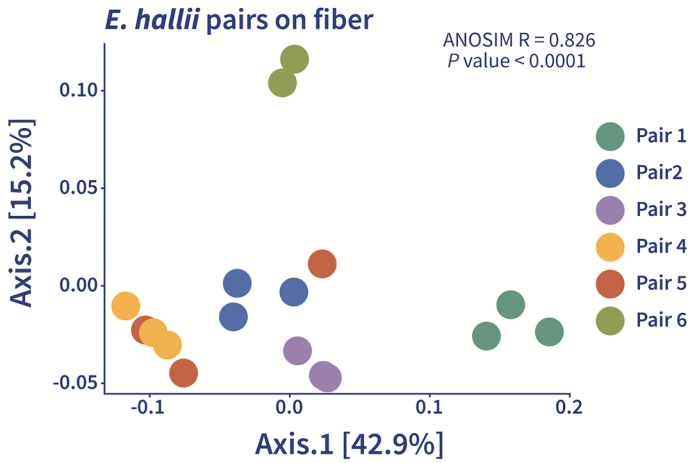

Extended Data Fig. 6 | Distinct proteomic responses of *E. hallii* across pairwise communities on fiber. PCoA of the overall proteomes (LFQ values) for *E. hallii* with various bacterial partners (triplicate biological cultures are indicated by distinct color scheme). Clustering analysis of expressed proteins according to the type of culture was performed using the ANOSIM test (two-sided) with 10000 randomizations of the data and the resulting R and *P* values are indicated.

https://doi.org/10.1038/s41564-026-02310-w

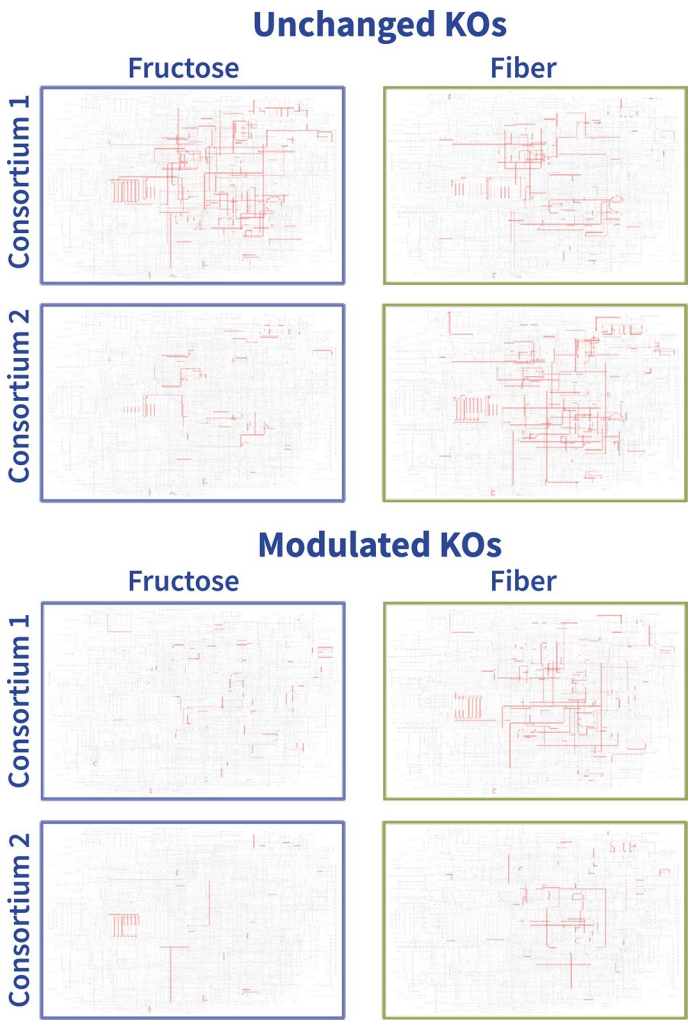

Extended Data Fig. 7 | Broad distribution of unchanged and modulated KO across metabolic pathways. KEGG metabolic pathway diagrams (map01100) for two different four-species consortia grown on either fructose or fiber. Each panel displays the KEGG pathway map generated using KEGG Mapper, with either unchanged or modulated KOs highlighted in red. The maps illustrate that that in all four consortia both unchanged and modulated KOs are broadly distributed across the metabolic landscape, with no repetitive patterns or consistent clustering or enrichment within specific sub-pathways.

https://doi.org/10.1038/s41564-026-02310-w

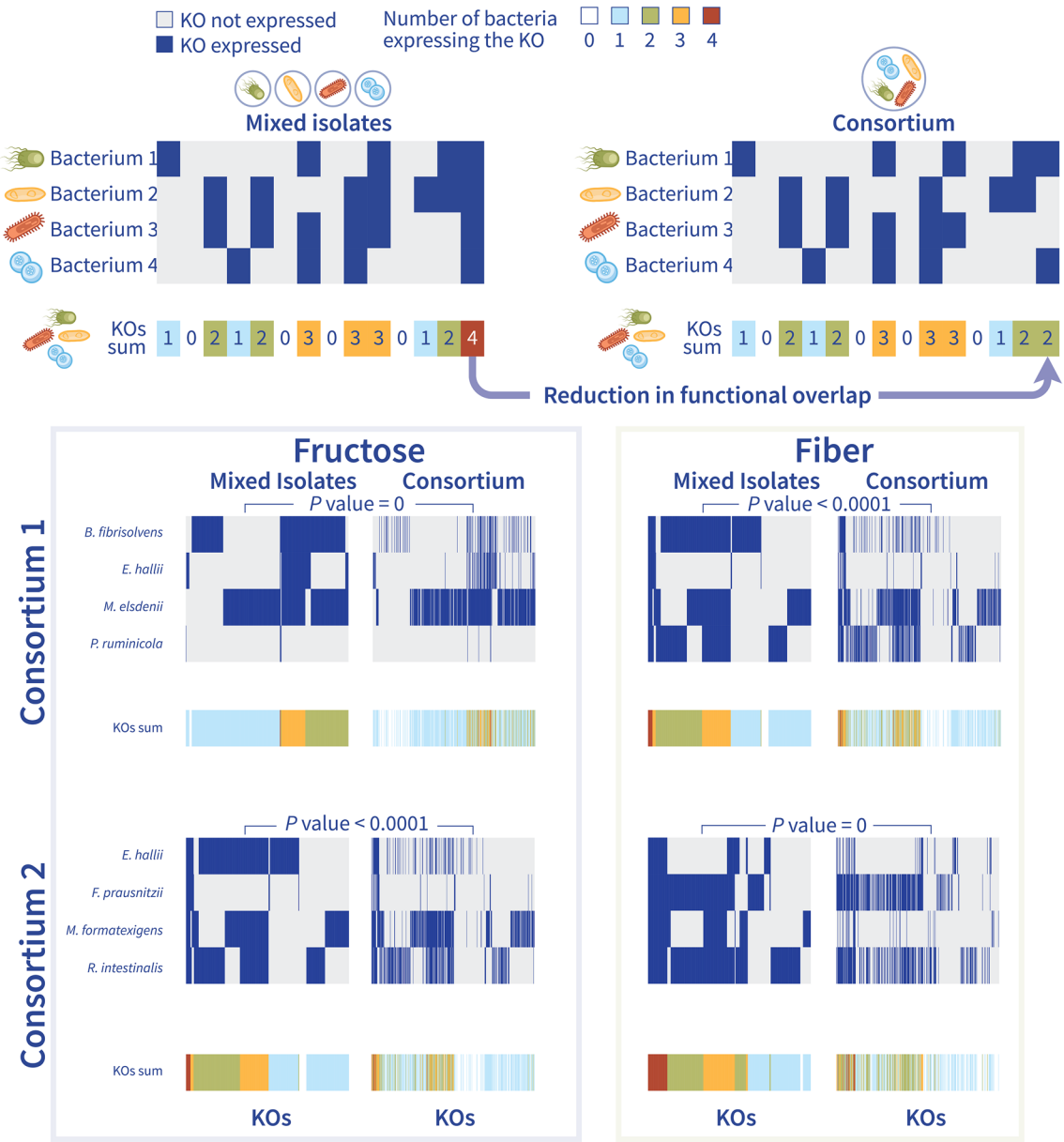

Extended Data Fig. 8 | Reduction in functional redundancy within four-species consortia compared to mixed isolates controls (LFQ presence-absence). Heatmaps of KOs within metabolic pathways (map01100) for two different four-species consortia grown on either fructose or fiber, alongside their corresponding mixed-isolate controls. Each heatmap represents the number of detected KOs per species in at least one of the three biological replicates (4 rows) and the total number of KOs detected across the entire consortium (bottom row). Comparisons reveal a marked reduction in functional redundancy within the grown consortia, as they exhibit fewer shared KOs than expected from the mixed isolates proteomic analyses. Chi-square test (two-sided) *P* values are indicated.

https://doi.org/10.1038/s41564-026-02310-w

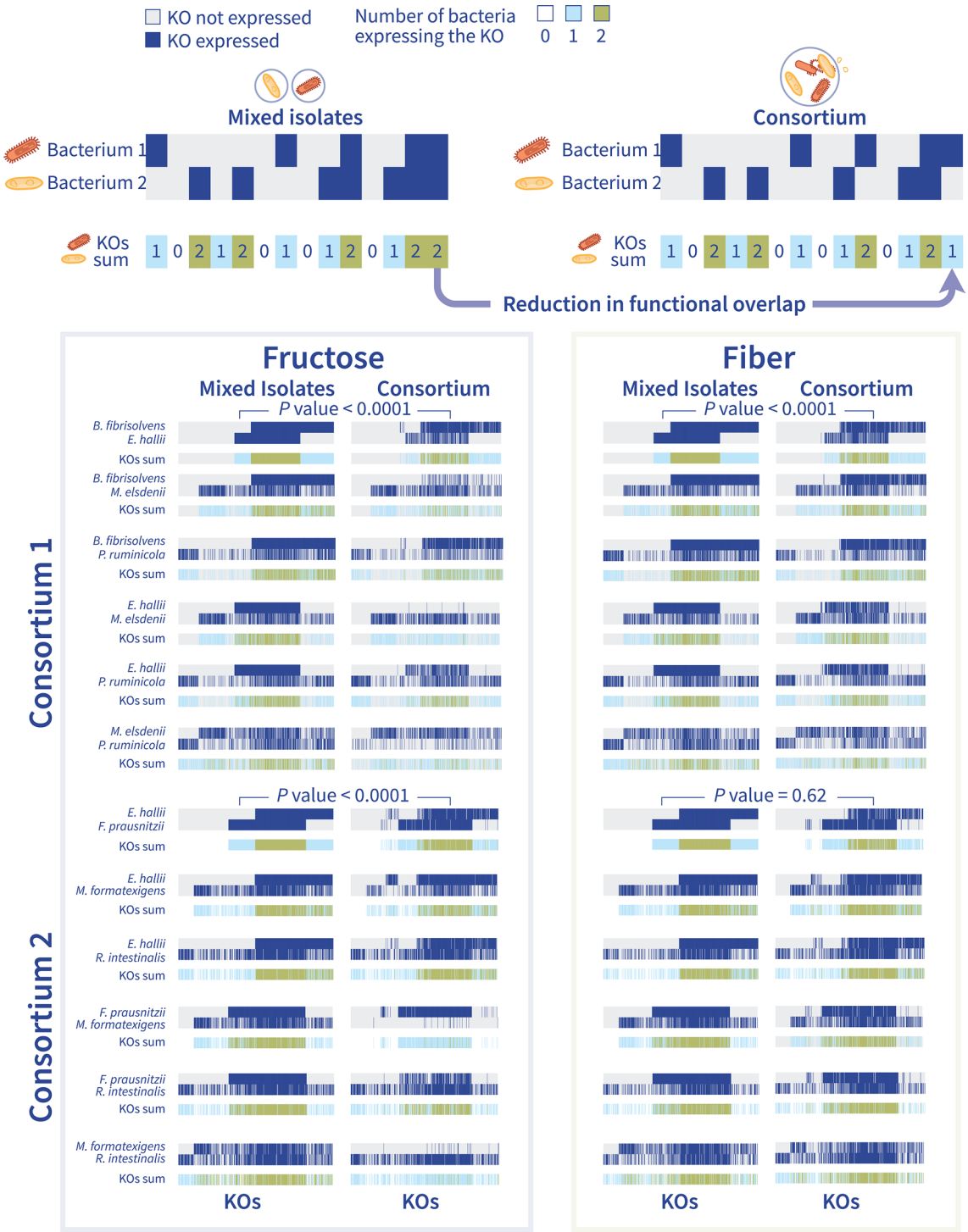

Extended Data Fig. 9 | Reduction in functional redundancy within pairwises consortia compared to isolates (LFQ presence-absence). Heatmaps of KOs within metabolic pathways (map01100) for all pairwises consortia grown on either fructose or fiber, alongside their corresponding isolates. Each heatmap represents the number of detected KOs per species in at least one of the three biological replicates (2 rows) and the total number of KOs detected across the entire consortium (bottom row). Comparisons reveal a marked reduction in functional redundancy within the grown consortia, as they exhibit fewer shared KOs than expected from the mixed isolates proteomic analyses. Chi-square test (two-sided) *P* values are indicated.

https://doi.org/10.1038/s41564-026-02310-w

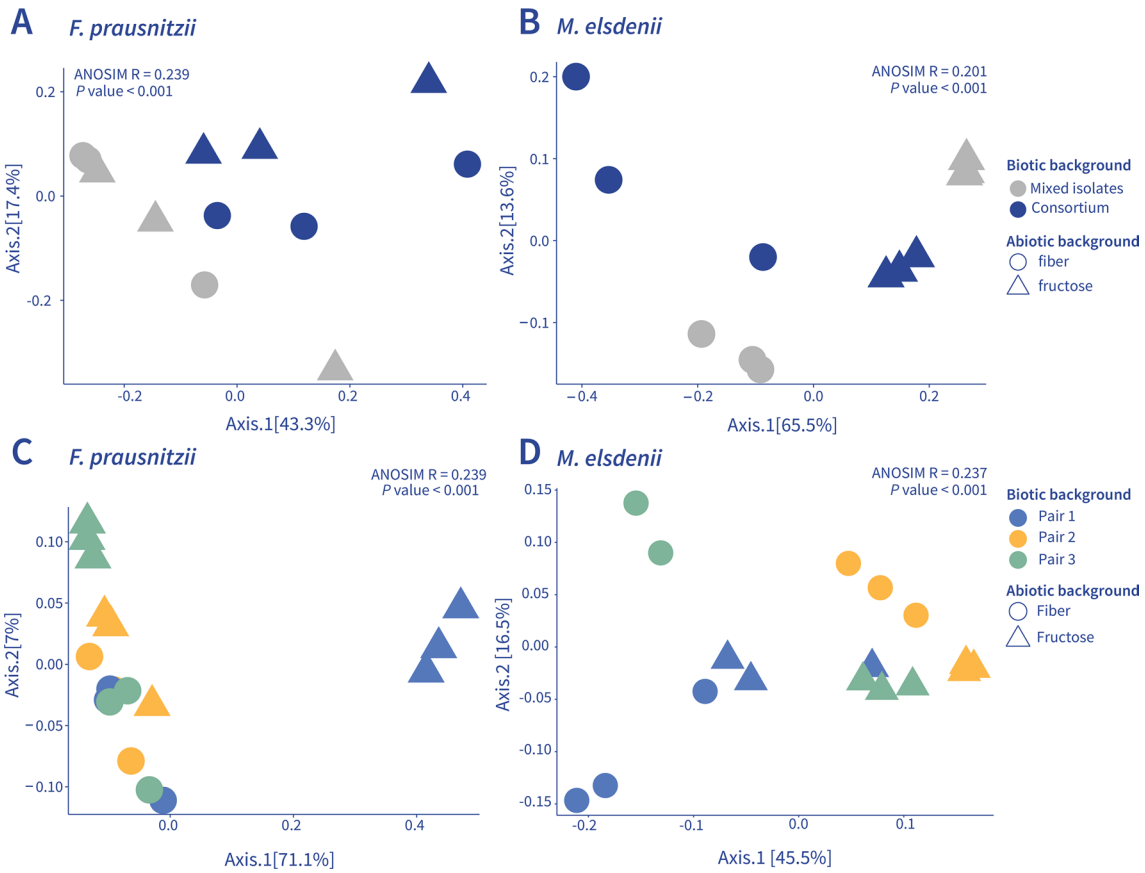

Extended Data Fig. 10 | Biotic factors drive the majority of proteomic variation in *F. prausnitzii* and *M. elsdenii*. PCoA for *F. prausnitzii* (**a** and **c**) and *M. elsdenii* (**b** and **d**), for the overall predicted proteomes (LFQ values) in grown consortia (in blue) or mixed isolates (in grey) for both carbon sources (represented by circles and triangles) in A and B, and for overall proteomes with various bacterial partners for both carbon sources (represented by circles and triangles) in C and D. In all panels, triplicate biological cultures are indicated by distinct color scheme and clustering analysis of expressed proteins according to the type of culture was performed using the ANOSIM test (two-sided) with 10000 randomizations of the data and the resulting R and *P* values corrected using FDR Benjamini–Hochberg are indicated.

nature portfolio

Corresponding author(s): Itzhak Mizrahi

Last updated by author(s): Feb 1, 2026

Reporting Summary

Nature Portfolio wishes to improve the reproducibility of the work that we publish. This form provides structure for consistency and transparency in reporting. For further information on Nature Portfolio policies, see our Editorial Policies and the Editorial Policy Checklist.

Statistics

For all statistical analyses, confirm that the following items are present in the figure legend, table legend, main text, or Methods section.

n/a	Confirmed	
☐	☒	The exact sample size (*n*) for each experimental group/condition, given as a discrete number and unit of measurement
☐	☒	A statement on whether measurements were taken from distinct samples or whether the same sample was measured repeatedly
☐	☒	The statistical test(s) used AND whether they are one- or two-sided *Only common tests should be described solely by name; describe more complex techniques in the Methods section.*
☒	☐	A description of all covariates tested
☐	☒	A description of any assumptions or corrections, such as tests of normality and adjustment for multiple comparisons
☐	☒	A full description of the statistical parameters including central tendency (e.g. means) or other basic estimates (e.g. regression coefficient) AND variation (e.g. standard deviation) or associated estimates of uncertainty (e.g. confidence intervals)
☐	☒	For null hypothesis testing, the test statistic (e.g. *F*, *t*, *r*) with confidence intervals, effect sizes, degrees of freedom and *P* value noted *Give P values as exact values whenever suitable.*
☒	☐	For Bayesian analysis, information on the choice of priors and Markov chain Monte Carlo settings
☒	☐	For hierarchical and complex designs, identification of the appropriate level for tests and full reporting of outcomes
☒	☐	Estimates of effect sizes (e.g. Cohen's *d*, Pearson's *r*), indicating how they were calculated

Our web collection on statistics for biologists contains articles on many of the points above.

Software and code

Policy information about availability of computer code

Data collection	For proteomic data collection: LTQ Orbitrap Velos Pro, LTQ Orbitrap XL / LTQ Orbitrap, LTQ Orbitrap Elite
Data analysis	For proteomic data analysis: NSAF: Mascot (v2.7.0.1), Scaffold (v. 5.0.1), X!Tandem (v. 2017.2.1.2), Peptide Prophet algorithm LFQ: FragPipe (v23.0), MSFragger (v4.3), MSBooster, Percolator,Philosopher (v5.1.1), IonQuant (v.1.11.11) vegan R package, KEGG database

For manuscripts utilizing custom algorithms or software that are central to the research but not yet described in published literature, software must be made available to editors and reviewers. We strongly encourage code deposition in a community repository (e.g. GitHub). See the Nature Portfolio guidelines for submitting code & software for further information.

Data

Policy information about availability of data

All manuscripts must include a data availability statement. This statement should provide the following information, where applicable:

- Accession codes, unique identifiers, or web links for publicly available datasets
- A description of any restrictions on data availability
- For clinical datasets or third party data, please ensure that the statement adheres to our policy

The mass spectrometry proteomics data have been deposited in the ProteomeXchange Consortium via the PRIDE partner repository (73) with the dataset identifiers PXD071838, PXD072222 and PXD073583.

Research involving human participants, their data, or biological material

Policy information about studies with human participants or human data. See also policy information about sex, gender (identity/presentation), and sexual orientation and race, ethnicity and racism.

Reporting on sex and gender	n/a
Reporting on race, ethnicity, or other socially relevant groupings	n/a
Population characteristics	n/a
Recruitment	n/a
Ethics oversight	n/a

Note that full information on the approval of the study protocol must also be provided in the manuscript.

Field-specific reporting

Please select the one below that is the best fit for your research. If you are not sure, read the appropriate sections before making your selection.

☒ Life sciences ☐ Behavioural & social sciences ☐ Ecological, evolutionary & environmental sciences

For a reference copy of the document with all sections, see nature.com/documents/nr-reporting-summary-flat.pdf

Life sciences study design

All studies must disclose on these points even when the disclosure is negative.

Sample size	Sample sizes were selected based on the minimum accepted standards in the field to ensure statistical validity while remaining feasible given the time-intensive processing required for metaproteomics (3 biological replicates).
Data exclusions	no data was excluded from the analyses
Replication	all replications were successful
Randomization	Randomization was not applied, as all samples were processed simultaneously using identical protocols, thereby reducing the risk of technical variability.
Blinding	Given the exploratory nature of the study and limited scale, blinding was not deemed necessary. All analyses followed standardized, unbiased workflows.

Reporting for specific materials, systems and methods

We require information from authors about some types of materials, experimental systems and methods used in many studies. Here, indicate whether each material, system or method listed is relevant to your study. If you are not sure if a list item applies to your research, read the appropriate section before selecting a response.

Materials & experimental systems

n/a	Involved in the study
☒	☐ Antibodies
☒	☐ Eukaryotic cell lines
☒	☐ Palaeontology and archaeology
☒	☐ Animals and other organisms
☒	☐ Clinical data
☒	☐ Dual use research of concern
☒	☐ Plants

Methods

n/a	Involved in the study
☒	☐ ChIP-seq
☒	☐ Flow cytometry
☒	☐ MRI-based neuroimaging

Plants

Seed stocks: n/a

Novel plant genotypes: n/a

Authentication: n/a